To the Graduate Council:

I am submitting herewith a thesis written by Clifford Lewis Ratliff entitled "The Study of Karman Vortex Shedding for Elliptical and Rectangular Cylinders." I have examined the final copy of this thesis for form and content and recommend that it be accepted in partial fulfillment of the requirements for the degree of Master of Science, with a major in Aerospace Engineering.

AHMAD D. VAKILI

Dr. Ahmad D. Vakili, Major Professor

We have read this thesis
and recommend its acceptance:

Roger Crawford

John E. Carruthers

Accepted for the Council:

Lew Winkel

Vice Provost and
Dean of The Graduate School

STATEMENT OF PERMISSION TO USE

In presenting this thesis in partial fulfillment of the requirements for a Master's degree at The University of Tennessee, Knoxville, I agree that the Library shall make it available to borrowers under rules of the Library. Brief quotations from this thesis are allowable without special permission, provided that accurate acknowledgment of the source is made.

Request for permission for extensive quotation from or reproduction of this thesis in whole or in parts may be granted by the copyright holder.

Signature Clifford L. Ratliff

Date 8/13/91

THE STUDY OF KARMAN VORTEX SHEDDING FOR ELLIPTICAL AND RECTANGULAR CYLINDERS

A Thesis

Presented for the

Master of Science

Degree

The University of Tennessee, Knoxville

Clifford Lewis Ratliff

December 1991

Copyright © Clifford Lewis Ratliff, 1991

All rights reserved

DEDICATION

I would like to dedicate my thesis to my devoted wife, Michelle W. Ratliff, who supported my many hours of work with her love, encouragement, and motivation while completing her thesis and carrying our first child - THANKS!. An additional dedication to my parents, Mr. William L. and Barbara H. Ratliff, for their love and motivation to help me complete my thesis no matter what obstacles were encountered.

ACKNOWLEDGEMENTS

I would like to thank my thesis advisor, Dr. Ahmad Vakili, for his patience and guidance he continuously exhibited during the preparation of the thesis. I would like to also acknowledge Dr. John Caruthers and Dr. Roger Crawford for their suggestions and insights during my thesis studies and participating on my thesis committee.

Special thanks is also extended to UTSI for the use of their research facilities and Calspan Corporation / AEDC Division for financially supporting my thesis studies. Both organizations allowed me to take advantage of the opportunity to further my education. A many thanks also go to my co-workers at Calspan and the UTSI test facility technicians for their encouragement and endless support.

Most importantly, I thank God for giving me the strength to complete this thesis and everything else in my life.

ABSTRACT

Vortex shedding frequencies were measured experimentally with a hot film anemometer behind elliptical and rectangular cylinders at 0, 30, 60, and 90 deg angles of attack between Reynolds number of approximately 2000 and 23000. The ellipses were of eccentricity 0.650, 0.866, and 0.950 with the rectangles cross section width to length ratio of 0.760, 0.500, and 0.312. Vortex shedding frequencies in the near wake of these cylinders were analyzed by means of the non-dimensional Strouhal number. The Strouhal number was presented in terms of a reference length based upon the cylinders projected frontal width and a near wake formation region length and compared to the accepted Strouhal number of 0.21 for circular cylinders in the irregular Reynolds number range. A near wake formation region reference length was extracted from flow visualization measurements in a water tunnel and used to calculate a universal Strouhal number for the elliptical cylinders between Reynolds number 2200 and 7200 and rectangular cylinders between Reynolds number 2200 and 8900. Obtaining a universal Strouhal number for the rectangular cylinders was unsuccessful, but a universal Strouhal number of approximately 0.3 was determined for the elliptical cylinders.

TABLE OF CONTENTS

SECTION PAGE

I. INTRODUCTION 1

II. EXPERIMENTAL APPARATUS AND METHOD 8
- 2.1 Water Tunnel 8
- 2.2 Low Speed Wind Tunnel 9
- 2.3 Test Articles 11
- 2.4 Instrumentation 12

III. VORTEX FORMATION PROCESS 14
- 3.1 Circular Cylinder 14
- 3.2 Elliptical Cylinder 19
- 3.3 Rectangular Cylinder 22

IV. RESULTS AND DISCUSSIONS 23
- 4.1 Freestream Velocity Verification 23
- 4.2 Strouhal Number Uncertainty Estimates 23
- 4.3 Strouhal Number Measurements 25
- 4.4 Universal Strouhal Number Measurements 64

V. GEOMETRIC INTERPRETATION OF STROUHAL NUMBER 72

VI. CONCLUSIONS 77

LIST OF REFERENCES 79

APPENDICES 82

APPENDIX A. ADDITIONAL READINGS 83

APPENDIX B. ESTIMATED STROUHAL NUMBER UNCERTAINTY EQUATION 86

VITA 88

LIST OF FIGURES

FIGURE PAGE

1. St versus REd curve for circular cylinders.....3
2. Model cross section details.....4
3. General layout of the UTSI Water Tunnel Facility....10
4. Typical installation in the UTSI Water Tunnel 13
5. Development of near wake vortex shedding 15
6. Laminar separation location (S) for ellipses 21
7. Estimated St number uncertainties.....26
8. Strouhal-Reynolds number relationship for unyawed circular cylinders.....30
9. Formation region behind bluff bodies.....33
10. St variation with REd for e=0.650.....35
11. St variation with Alpha for e=0.650.....36
12. St variation with REd for e=0.866.....39
13. St variation with Alpha for e=0.866.....40
14. Water and wind tunnel St comparison for e=0.866.....42
15. St variation with REd for e=0.950.....44
16. St variation with Alpha for e=0.950.....46
17. Comparison of St for ellipses at zero Alpha.....47
18. Comparison of St for ellipses at 30 deg Alpha.....48
19. Comparison of St for ellipses at 60 deg Alpha.....49
20. Comparison of St for ellipses at 90 deg Alpha.....50
21. St variation with REd for rectangle b/a=0.760.....53
22. St variation with Alpha for rectangle b/a=0.760.....54

FIGURE PAGE

23. St variation with REd for rectangle b/a=0.500.....55

24. St variation with Alpha for rectangle b/a=0.500.....56

25. St variation with REd for rectangle b/a=0.312.....57

26. St variation with Alpha for rectangle b/a=0.312.....58

27. Comparison of St for rectangular and circular cylinders at zero Alpha 60

28. Comparison of St for rectangular and circular cylinders at 30 deg Alpha 61

29. Comparison of St for rectangular and circular cylinders at 60 deg Alpha 62

30. Comparison of St for rectangular and circular cylinders at 90 deg Alpha 63

31. Photographs of near wake vortices at REd=2452.....65

32. St based on d and dw for elliptical cylinders.....69

33. Variation of dw/d with e from 0 to 90 deg Alpha.....70

34. St based on d and b for the ellipses.....73

35. Variation of d with Alpha for the ellipses.....74

36. St based on d and b for the rectangles.....75

37. Variation of d with Alpha for the rectangles.....76

LIST OF TABLES

TABLE PAGE

1. Experimental water and wind tunnel St data 27

2. Experimental calculation of St based on dw 71

LIST OF SYMBOLS

SYMBOLS

a,c	Constant cylindrical length dimension parallel to freestream at zero alpha (α), in.
b,h	Constant cylindrical width dimension perpendicular to freestream at zero alpha, in.
Cd	Form drag coefficient
d	Projected frontal surface width dimension relative to freestream for varying alpha, in. ellipse: $d=\sqrt{[b^2\cos^2\alpha+a^2\sin^2\alpha]}$ rectangle: $d=\sqrt{[b\cos\alpha+a\sin\alpha]}$
dw	Lateral distance across the near wake of a bluff cylinder measured between the inner most wake boundary or streak line, in.
D	Test section width at cylinder location, in.
e	Eccentricity of the elliptical cylinders, $e=\sqrt{[1-(b/a)^2]}$
f,f	Vortex shedding frequency aft of a bluff cylinder from one shear layer, Hz
F	Non-dimensional shedding frequency, fd^2/τ
l'	Semi-arc length of a cylinder cross section, in.
m	Tunnel blockage correction factor, $m\approx1+1.25(d/D)$
REd	Reynolds number based on d, $\sigma Ud/\mu$
S	Cylinder separation location defined by x/l'
Sl	Lower separation location
St	Strouhal number based on d, fd/U
St()	Strouhal number based on (), where ()=d or b
St'	Universal Strouhal number, fdw/U
Su	Upper separation location

u'	Potential velocity along cylinder surface, in./sec
U	Freestream velocity upstream of cylinder, in./sec
x,y,z	Orthogonal reference axes measured from center of cylinder base, in.
α	Cylinder angle of attack relative to U with the rotation about the z-axis, deg
σ	density, lbm/in.^{3}
μ	Absolute viscosity, lbf/in.-sec
τ	Kinematic viscosity, in.^{2}/sec
δ	Boundary-layer thickness, in.

I. INTRODUCTION

The relation between vortex shedding frequency and the freestream velocity were first demonstrated by Strouhal in 1878 [1]. Since 1878 many other investigators have been intrigued with the periodic motion of vortex-street patterns downstream of different body geometries over a broad range of Reynolds number. The first pictures showing the alternating pattern of vortices in the wake were published by Ahlborn in 1902 [2]. Karman gave his famous theory of vortex street in 1911 [3], increasing the scientific communities awareness to study the subject further. Today the mechanism of vortex shedding is still not fully understood and research continues. Investigations of vortex shedding tend to concentrate more on understanding the "product" of the mechanism via flow visualization techniques. This research also concentrated on the vortex shedding phenomenon, but in an effort to provide additional data towards determining the source of the vortex mechanism. Additional readings concerning vortex shedding with different objectives than the current study is presented in Appendix A.

The objective of this study was to obtain and compare near-wake vortex shedding frequencies of stationary

noncircular cylinders at angle of attack between Reynolds number (REd=σUd/μ) 2000 and 20000 with the classical Strouhal (St=fd/U) versus Reynolds number curve for circular cylinders as referenced in Roshko [4]. Figure 1 represents the classical Strouhal number curve varying with Reynolds number for different cylinder diameters.

The bodies selected consisted of elliptical and rectangular cross section cylinders. The three ellipses used for the investigation consisted of eccentricity (e) 0.650, 0.866, and 0.950 which span between the circular cylinder (e=0) and the flat plate (e=1). The major axis of the ellipse was held constant for all elliptical models while the minor axis dimension was changed. The rectangular cylinder width (2b) and length (2a) dimensions are identical as the major and minor axis dimensions of the ellipses. The rectangles are defined by width to length (b/a) ratios of 0.312, 0.500, 0.760 and all have sharp corners. The dimensions were selected to control the Reynolds number (REd), where d is the cylinder projected frontal width, between 2000 and 20000 based on the water and wind tunnel operating envelope. Operating in this irregular Reynolds number range [4] (300<REd<10000+) the shedding frequencies could be compared with the circular cylinder Strouhal number of approximately constant value 0.21 as presented in Fig. 1. Figure 2 presents the

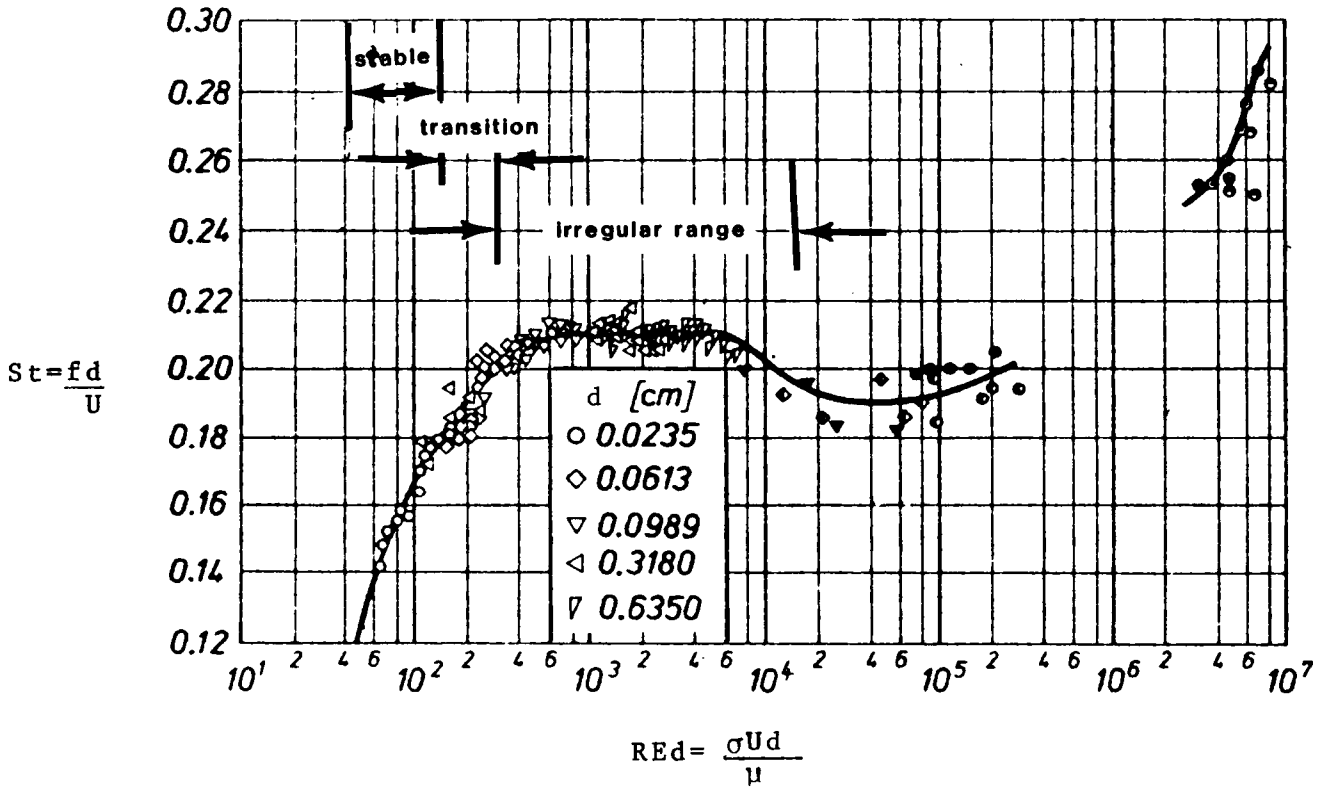

Figure 1. St versus REd curve for circular cylinders [5]

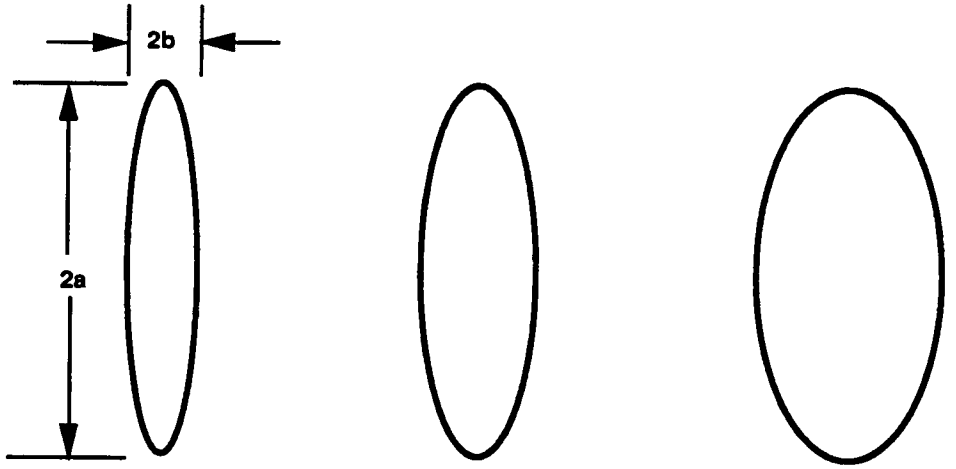

e=0.95
2a=1.000 in.
2b=0.312 in.

e=0.866
2a=1.000 in.
2b=0.500 in.

e=0.65
2a=1.000 in.
2b=0.760 in.

a. Elliptical Cross Sections

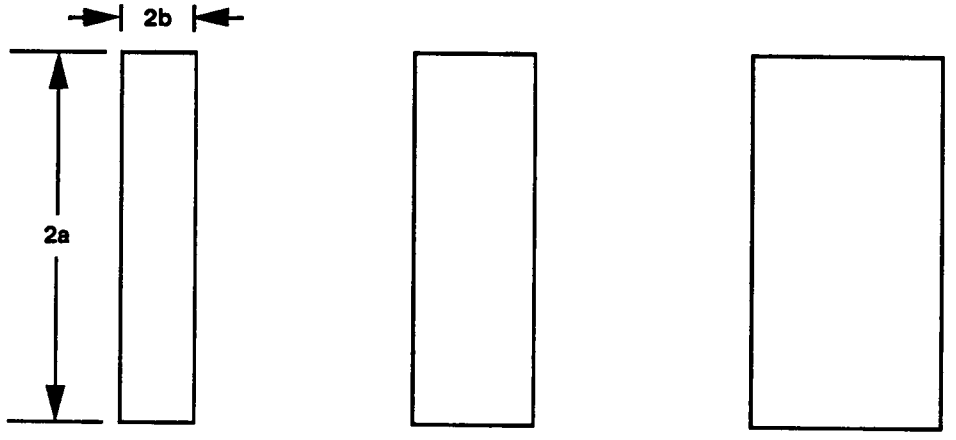

b/a=0.312

b/a=0.500

b/a=0.760

b. Rectangle Cross Sections

Figure 2. Model cross section details

the cross sectional details of the elliptical and rectangular cylinders for comparison.

The Strouhal number is a dimensionless parameter relating vortex shedding frequency (f), reference length (d), and freestream flow velocity (U). Roshko [6] and Gerrard [7] consider shedding frequency to depend on the scale of the formation region or coupling region such that if the shear layers are brought closer together in the first few body diameters the vortex interaction is increased in a shorter amount of time. The size of the formation region in the near wake of the cylinder is dependent upon the projected frontal width (d) and "bluffness" of the cylinder immersed in the flow. Bluffness of a cylinder is based upon the width of the wake shear layer compared to the cylinder dimension. So, bluffer cylinders cause the flow to diverge more creating a larger wake and having larger drag [6]. According to these statements and the definition of Strouhal number, as d increases the shedding frequency decreases. This study will demonstrate the following: 1) Strouhal number decreases with increasing bluffness for elliptical cylinders, 2) Strouhal number for ellipses is higher than circular cylinders over a wide range of eccentricity and angle of attack, 3) Strouhal number increases with increasing bluffness for rectangular cylinders, 4) shedding

frequency measurements in a water and wind tunnel could be duplicated, and 5) a "universal" Strouhal number was determined for elliptical cylinders for eccentricity 0.650, 0.866, and 0.950.

Universal Strouhal number for bluff bodies, derived by Bearman [8], was based upon vortex shedding frequency, longitudinal vortex spacing, and the outer wake boundary velocity associated with base pressure coefficient. The present study determined a universal Strouhal number (St') based on vortex shedding frequency (f), near-wake free shear layer separation distance (dw), and the freestream flow velocity (U). Fage and Johansen [9] investigated the structure of free shear layers behind a circular cylinder and determined St'≈0.28 at REd=20000 using dw. The use of longitudinal vortex spacing as a reference length was not well defined in the irregular Reynolds number range especially at non-zero angles of attack because of turbulent vortex "burst" and thus was not a viable method. Determining an outer wake boundary velocity via base pressure measurements was not attempted since longitudinal vortex spacing was not well defined as mentioned. The universal Strouhal number defined in this study is simplified compared to Bearman, but will demonstrate to be applicable to elliptical cylinders and not rectangular cylinders. It is important to realize since the elliptical

and rectangular cylinders are two classes of shapes, the vortex formation process will be different and is explained further in Section III. Basically, the ellipse allows the separation points to oscillate because of the smooth radius of curvature and Reynolds number effects can be expected. For the rectangular shapes the separation points are fixed at the corners and should be insensitive to Reynolds number effects [10].

II. EXPERIMENTAL APPARATUS AND METHOD

2.1 Water Tunnel

The University of Tennessee Space Institute (UTSI) water tunnel is a continuous closed circuit facility flowing water in the horizontal plane. The test section measures 12 in. deep, 18 in. wide, and 60 in. long with 0.5 in. plexiglas sides except for the top which is an open surface. The plexiglas and open surfaces are ideal for observing and photographing the flow field. The facility is equipped with filters, aspirators and degas pipes. The stilling chamber is a cylindrical shaped steel tank which has a 60 in. outside diameter and is 112 in. long. There are four stainless steel screens and two aluminum honeycombs located inside. The length to diameter ratio of the honeycomb is 6. The tunnel was designed to give a turbulence level of 0.1% in the test section. The nozzle is a bell mouth that continuously changes from a circular shape to a rectangular shape with a contraction ratio of 13.5. In the first bend downstream of the test section, a portion of the main flow is bypassed through a filter to control the particle size in the tunnel to less than 10 microns. The propeller is connected to a continuously variable speed motor that is controlled by a resistive potentiometer.

The propeller is located at the second bend downstream

of the test section. The water velocity can be varied from 1 to 6 in/sec. The motor is mounted on a vibration isolated mount and is flexibly connected to the propeller shaft. The fluctuations in the test section because of propeller rotation are minimal. The characteristic frequency of the water tunnel is about 12 Hz. Above the test section floor is a smooth flat wood false floor mounted 1 in. above the bottom acting as a boundary layer splitter device. The sharp leading edge of the false floor is approximately 5 in. ahead of the model positioning hole. The general layout of the water tunnel facility is presented in Fig. 3.

2.2 Low Speed Wind Tunnel

The low speed wind tunnel facility at the UTSI has a test section dimension of 14 in. high x 20 in. wide x 42 in. long. It is an open circuit, continuous suction type wind tunnel with a closed test section. The tunnel is powered by a 55 in. diameter fan with a 75 HP motor. Test section velocities range from 10 to 300 ft/sec and is controlled by an IBM PC. The test section velocities are calculated using Bernoullis equation with the static and pitot pressure measurements at the entrance of the test section.

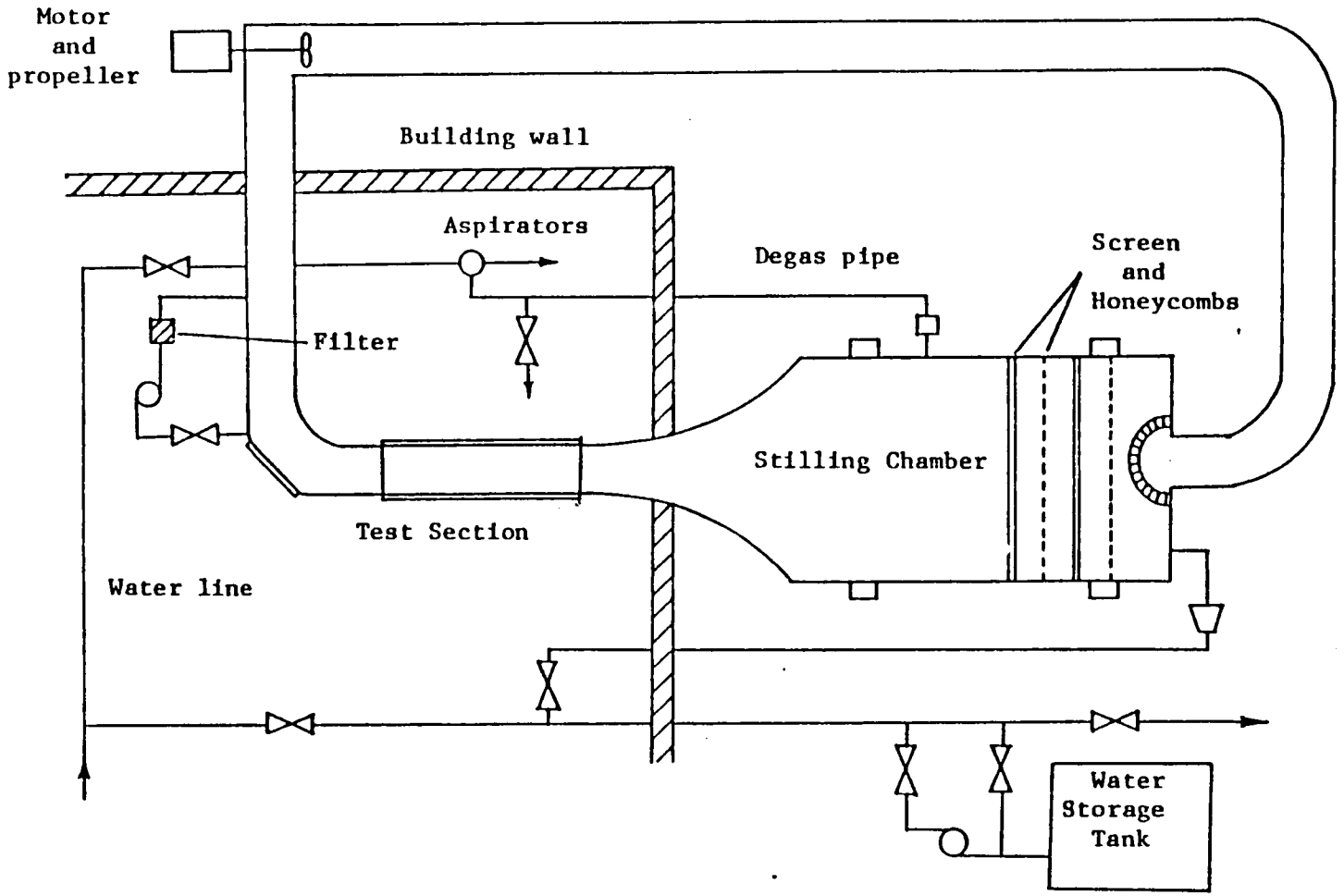

Figure 3. General layout of the UTSI Water Tunnel Facility

2.3 Test Articles

All test articles were machined from aluminum stock and were hand polished at the UTSI machine shop. Model dimensions were kept within a 0.002 in. tolerance. The elliptical models were cut using a template for reference. The coordinates for the template were computed from using the standard equation of an ellipse $[(x^2/a^2)+(y^2/b^2)=1]$. Each model has the same length of 11 in. with a 1 in. insertion dowel at the base of the model for positioning in the center of the test section floor. At the top are two locating pins which fit to a common adaptor. The adaptor was marked on the circumference at 0, 30, 60, and 90 deg to align with a zero degree scribe mark on a plexiglass mounting surface placed above the water channel for consistent orientation. The model angle of attack was varied by manually setting the adaptor at the prescribed locations.

The ellipse with e=0.866 was also tested in the wind tunnel to compare and to verify the observations made in the water tunnel. The ellipse was positioned in the wind tunnel test section similar to that of the water tunnel. Scribe marks of 0, 30, 60, and 90 deg were on the test section floor to align with the trailing edge of the ellipse. A splitter plate was placed on the top of the model since the test section vertical distance was greater

than the model length. The splitter plate was a 3 in. thin square plexiglass with two holes to fit over the locating pins. Installation sketches of a model in the water tunnel are presented in Fig. 4.

2.4 Instrumentation

Vortex-shedding frequencies were measured with a TSI constant-current hot-film anemometer (model#: 1212-60W, SN: 36300, TSI Ref.#: 54299) with the hot-film placed downstream of the models in the near wake (i.e. x=2d, y=-d) as presented in Figure 4. The output signals from the hot film were measured by a TSI Intelligent Flow Analyzer (IFA)-100. The frequency measurements were identified by a Hewlett Packard 3582A Spectrum Analyzer. A 30W Argon laser was used to scatter a horizontal plane of light across the induced fluorescent dye injected upstream of the models. The flow visualization photographs were obtained approximately 1 ft. above the test section using a Nikon 35mm camera with FS 5.6, shutter speed 1/30 sec and push processing 200 ASA EktaChrome Kodak to 800.

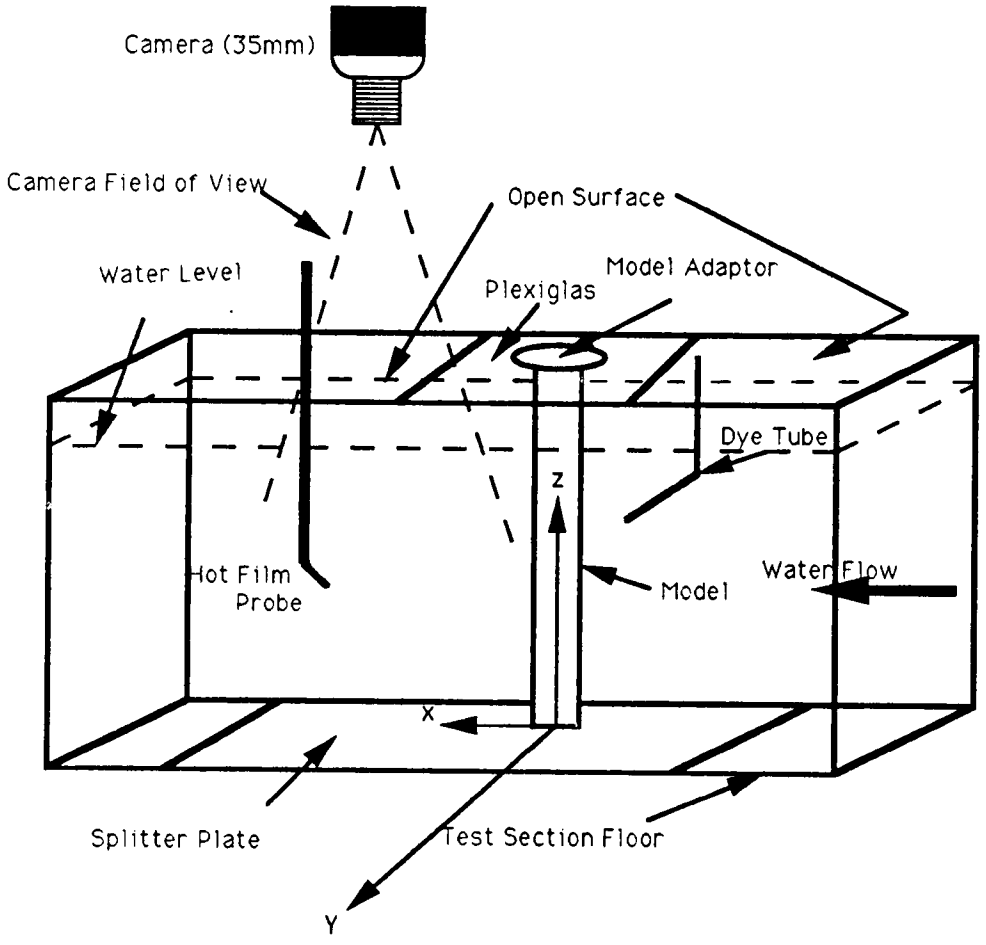

Figure 4. Typical installation in the UTSI Water Tunnel

III. VORTEX FORMATION PROCESS

Before discussing the results in Section IV, it will be beneficial to review the two-dimensional circular cylinder vortex formation process. Application of this information in association with the data will be useful in understanding the vortex formation process of the elliptical and rectangular cylinders of the current study.

3.1 Circular Cylinder

Suppose a circular cylinder is positioned in a uniform fluid beginning to move steady in one direction. At very low speeds (i.e. REd≈5) the fluid elements "sense" the approaching cylinder and are forced to deviate from an undisturbed uniform and straight line. The path of the fluid elements flow around the cylinders' surface. The streamlines are tangent to the cylinder surface originating from a forward stagnation point (U=0) on the cylinder as presented in Fig. 5a. The surrounding streamlines are no longer uniform, but a minimal amount of energy was lost during the process to approximately join again in the rear of the cylinder and cause a rearward stagnation point with minimal losses. The primary loss of fluid energy is transported through friction or shear stresses between the cylinder and flow resulting in a boundary layer profile. Also, the net surface pressure distribution is

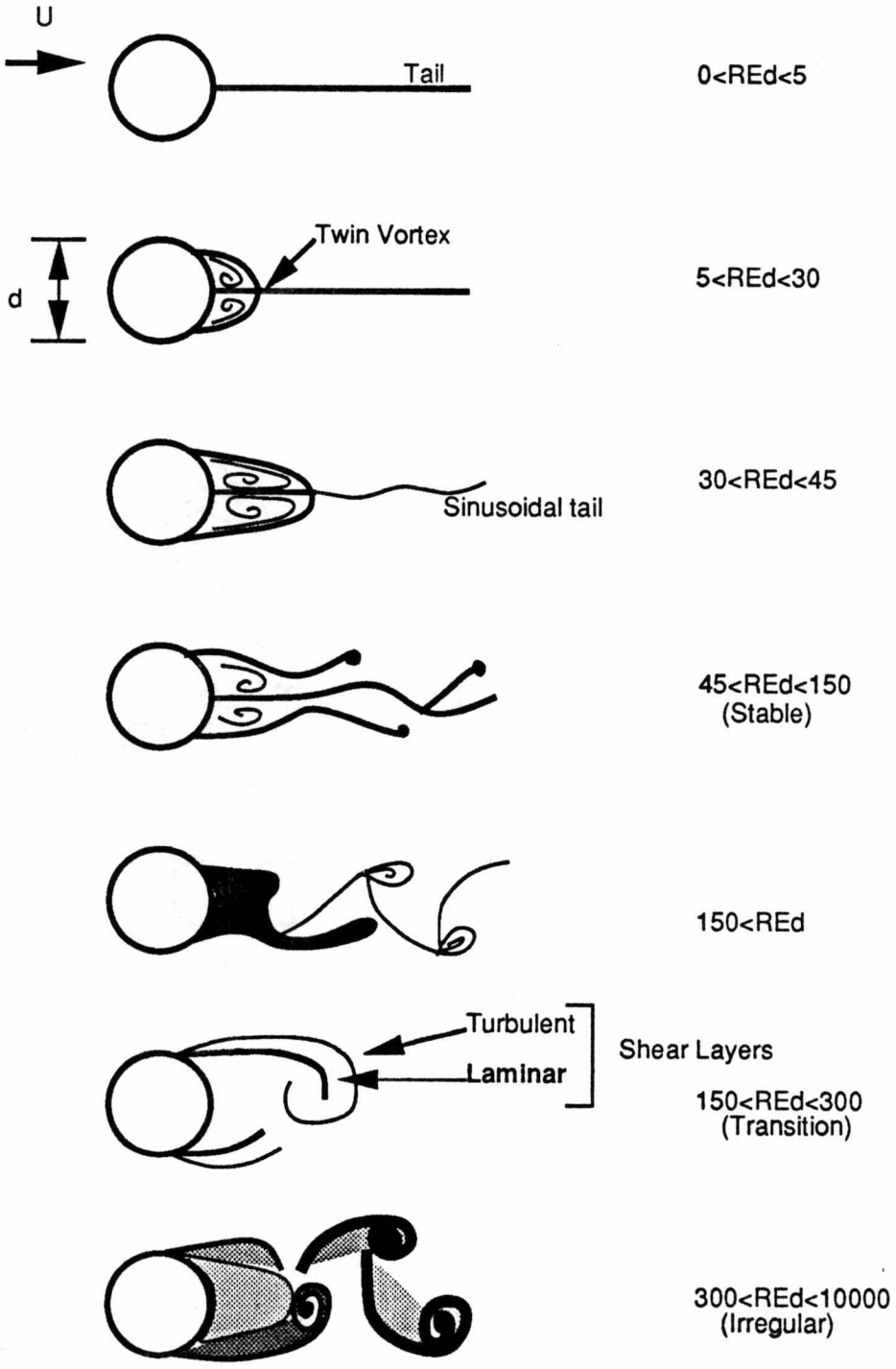

a. circular cylinder [4,10]

Figure 5. Development of near wake vortex shedding

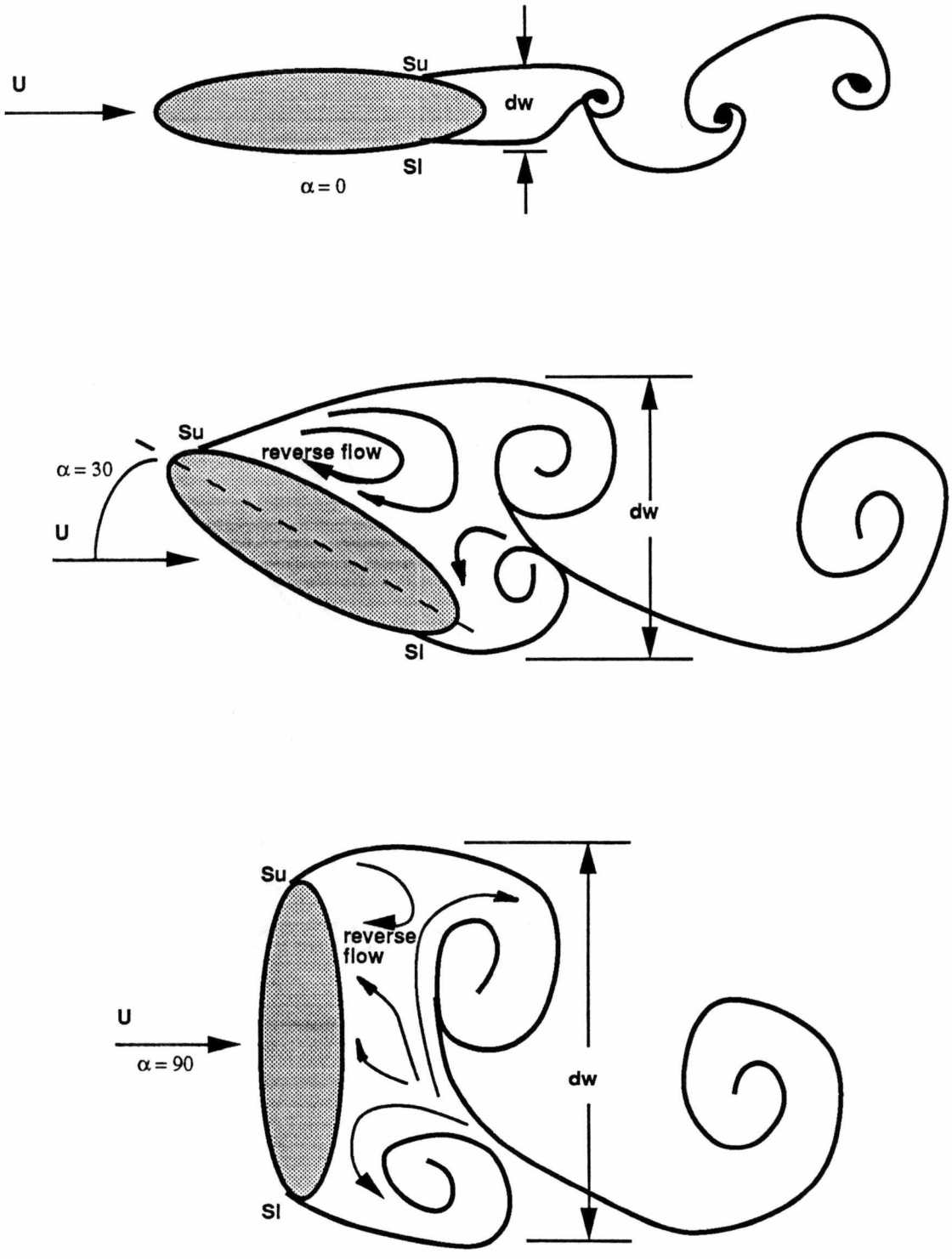

b. elliptical cylinders
Figure 5. (Continued)

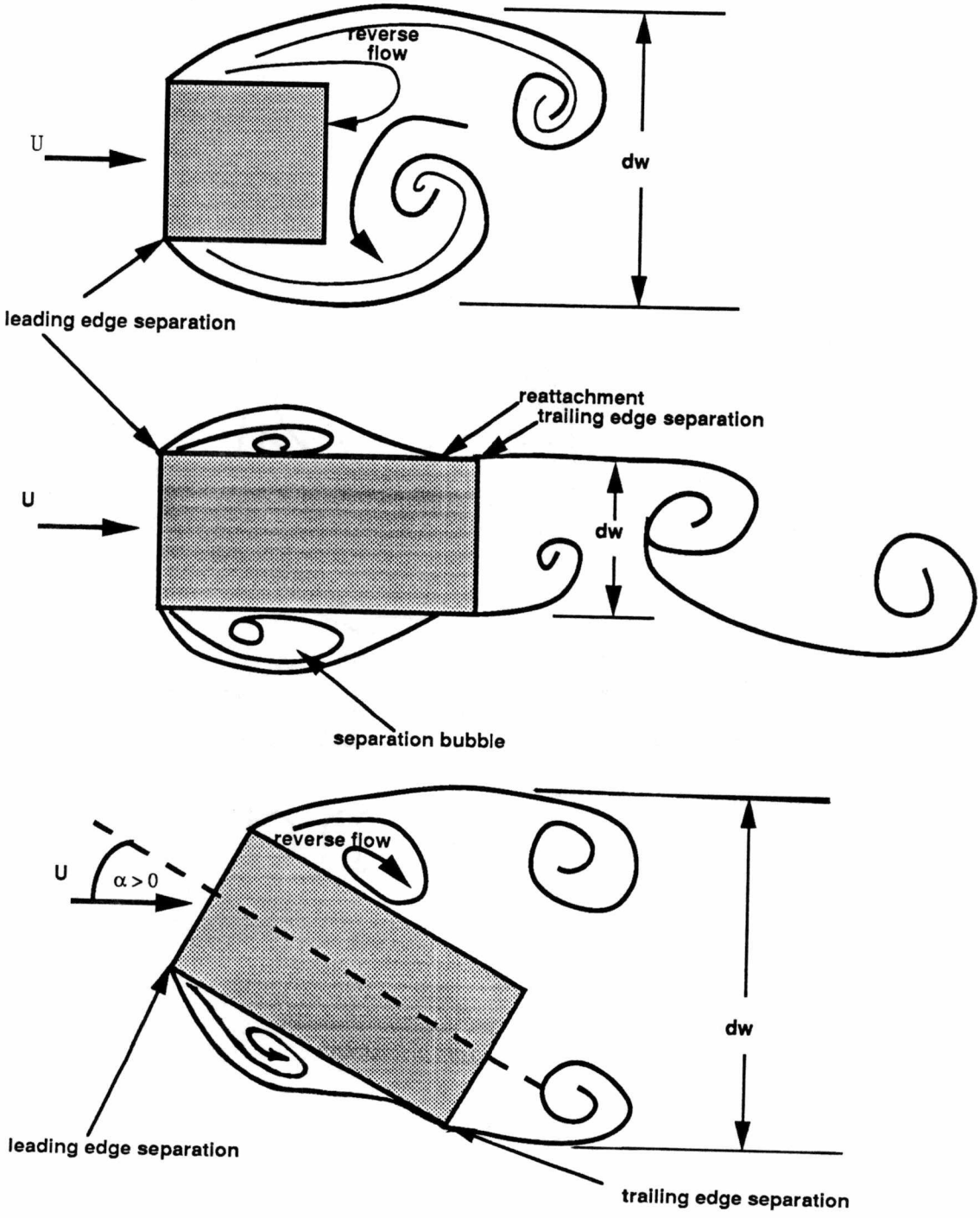

c. rectangular cylinders
Figure 5. (Concluded)

approximately zero resulting in approximately zero drag. At the rear stagnation point the streamlines continue downstream of the cylinder in a uniform profile similar to the upstream profile. With REd between 5 and 30, losses in the flow increase and the streamlines adjacent to the cylinder separate and fail to reach the rear of the cylinder. At this point the steady separated shear layer forms a closed region behind the cylinder termed "wake bubble boundary" forming twin vortices [11]. The wake-bubble boundary separates the external and recirculating flow at the base of the cylinder. The wake-bubble boundary is actually a streamline extending from the separation point on the cylinder to a wake stagnation point within the diameter of the cylinder along centerline. The downstream streamline (i.e. tail) along centerline is steady and straight. Increasing REd between 30 and 45 causes the separation point on the cylinder to move further upstream along the surface with the twin vortices enlarging and pushing the wake stagnation point outside the cylinder diameter. Here, the tail begins to oscillate indicating signs of instability are developing downstream. At REd between 45 and 150 (i.e. stable range) the classic Karman vortex street appears and the rear twin vortices are no longer defined. The vortices retain their pattern for many diameters downstream before decaying

through viscous diffusion [4]. The next Reynolds number range is the transition range, 150<REd<300, where laminar-turbulent shear layers (laminar separated boundary layer) "spring" from each separation point on the cylinder. The combination of the free layer and backflow behind the cylinder increase until sufficient circulation is established and then the fluid breaks away at regular intervals. Before the circulating fluid can break away it must become turbulent [4]. Therefore, each vortex spiraling downstream contains turbulent fluid. Once the transition has occurred, increasing REd into the irregular range (300<REd<10000) reduces the effects of vortex formation and vortex shedding remains constant. In the irregular range the vortex diffusion is turbulent rather than viscous as in the stable range.

3.2 Elliptical Cylinder

The vortex formation for elliptical cylinders is an extension of the circular cylinder with eccentricity of zero with similar features. An additional feature that the ellipse has that the circular cylinder does not have is variation with angle of attack. With the ellipse at zero alpha (major axis, 2a, parallel to the flow) the flow "senses" the cylinder, but is able to flow around the cylinder with less difficulty because of the streamlining contour. Streamlining is synonymous with body bluffness

when a body contour is such that it reduces the flow divergence. For a group of ellipses with increasing e at zero alpha (2a=constant) the cylinder decreases its bluffness thus allowing the external fluid to flow more efficient with less disturbance to the surrounding flow. With the slender elliptical cylinder the laminar separation location (S) moves aft on the body as presented in Fig. 6. Since the ellipse has contoured surfaces the separation point is able to oscillate and is more likely to be Reynolds number dependent. As the ellipse projected frontal width decreases the wake region reduces forcing the free shear layers closer together. With the free shear layers closer together the interaction time is reduced resulting in higher shedding frequencies. A slender ellipse will most likely require a higher Reynolds number than a circular cylinder, equal to the ellipse minor axis (2b), before the flow is sufficiently disturbed to produce vortex shedding. As the ellipse is rotated to higher angle of attack (maximum being 90 deg) the body bluffness increases causing the separation points to counter rotate. With increasing bluffness the wake width increases, thus reducing the shear layer interaction. With the shear layers further apart, than at zero alpha, the vortex shedding frequency decreases. Typical vortex flow patterns downstream of elliptical cylinders is presented in Fig. 5b.

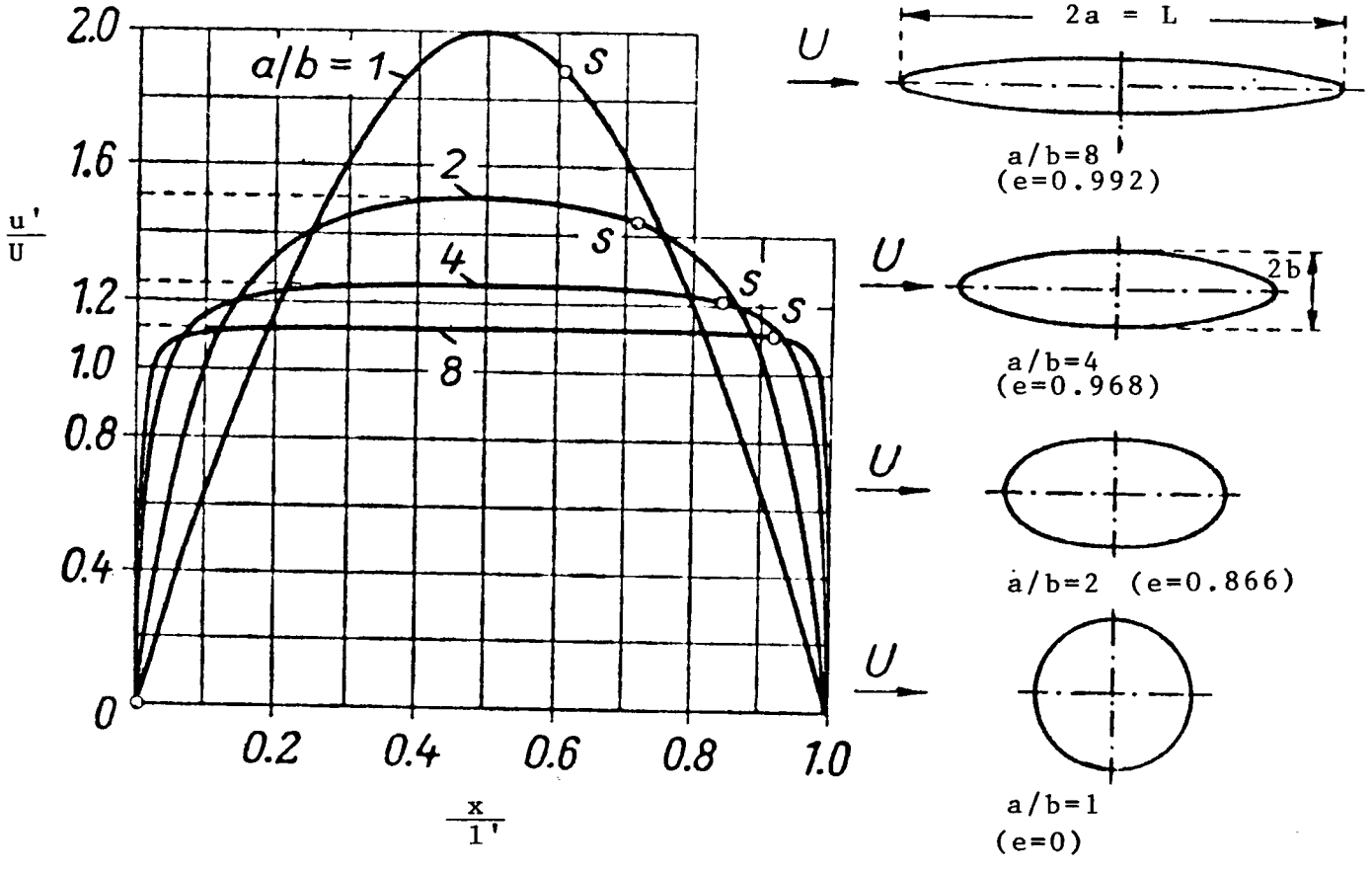

Figure 6. Laminar separation location (S) for ellipses [5]

3.3 Rectangular Cylinder

At low Reynolds numbers (i.e. REd<80) flow around a square cylinder (b/a=1) is known to separate at the trailing edge rather than the leading edge. With an increase in REd the separation moves to the leading edges and the vortex shedding decreases sharply with St=0.13. With an increase in angle of attack (≈13.5 deg) the sides become more exposed causing the shear layer to reattach, thus increasing the Strouhal number to a maximum value of 0.18 in the irregular range [12]. Also, if the cylinder were extended downstream enough at zero alpha the shear layers could reattach [12]. With the shear layers reattached the REd could be increased above 80 until separation occurred again at the leading edges. Once the rectangle is sufficiently rotated the sharp corners fix the separation points. The process is reversed as the cylinder is continuously rotated and the sides at zero alpha approach the oncoming flow at 90 deg. It's obvious that the separation points are fixed at the sharp corners, but what is unknown is when do they become effective (i.e. alpha, REd, and b/a). Typical vortex patterns around rectangular cylinders is presented in Fig. 5c.

IV. RESULTS AND DISCUSSIONS

4.1 Freestream Velocity Verification

Since the Strouhal number is determined from three parameters (i.e. f,d,and U) it was important to establish a method of determining the freestream velocity (U) of the water tunnel during each entry. Rather than assume the tunnel calibration for determining flow velocity the shedding frequency downstream of a reference circular cylinder (0.5 in. diam.) was measured in the near wake. Roshko [4] explains that by measuring the shedding frequency, knowing the circular cylinder diameter, and calculating the kinematic viscosity a dimensionless frequency, $F=fd^2/\tau$, is computed and is related to Reynolds number, thus the velocity can be calculated. At Reynolds number ranging from 300 to 10000 the maximum error, relative to a best-fit curve, is approximately 4 percent for F=0.212*REd-2.7. The Reynolds number range 300 to 10000+ is defined as irregular [4] and can vary because of configuration, free-stream turbulence, wall effects, and so forth. Eventhough the shedding range is irregular a predominant shedding frequency can be determined with consistent results [4].

4.2 Strouhal Number Uncertainty Estimates

When comparing data that has been obtained during an

experiment it is important to understand that a certain percentage of the measurement is in error. Errors in data measurements have to be accounted for to be able to decide if the data are invalid, acceptable, or inconclusive. Whether the error originates from an assumption that is required to obtain a solution for a computer computation or electronic limitations for measurement equipment the data would be meaningless without a "yardstick" for reference. The yardstick in this case is an uncertainty band composed of a bias and precision component. The uncertainty band is an estimate of how a perturbation error in a measurement can alter the final measurement from the "true" value. For example, a measurement was obtained several times and the value was the same, then the data is very repeatable and the percentage of error in precision is negligible. Still, this may not be the correct value because the bias component may be offset from the true value. There are many other senarios, but it is common practice to quote uncertainty estimates to bound typical data scatter.

For the current investigation an uncertainty analysis was performed by differentiating the Strouhal number equation and including a perturbation error through the equation as presented in Appendix B. The three major sources of errors possible are in the freestream velocity (U), reference diameter (d), and the frequency measurement

(f). Figure 7 presents a curve with a 4 percent error in U with the other two parameters equal to zero and another curve with additional error of 2 percent for d and f. A conservative two percent error in d (i.e. positioning the model) for the ellipse of eccentricity 0.650 and 0.950 results in approximately 1.2 deg and 5.4 deg respectively. A two percent error in positioning each of the rectangular models is approximately 1.5 deg. Based on the selected precision errors as presented in Figure 7 (bias is assumed to be zero) the Strouhal number uncertainty band for the ellipse data is approximately ±0.012 for Strouhal numbers of 0.25. Strouhal number uncertainties for the rectangle data is approximately ±0.010 for Strouhal numbers of 0.200 which translates to ±5 percent error in Strouhal number.

4.3 Strouhal Number Measurements

Experimental Strouhal data points were not presented in either a table or figure for the cylinder (0.5 in. diam.) because its use was strictly for determining tunnel velocity prior to measuring vortex shedding frequencies of the other models as explained in Section 4.1. Table 1 is presented with Strouhal numbers for only the ellipses and rectangles at their respective angles of attack. Typical Strouhal versus Reynolds number curve for unyawed circular cylinders with various diameters is presented in Figure 8.

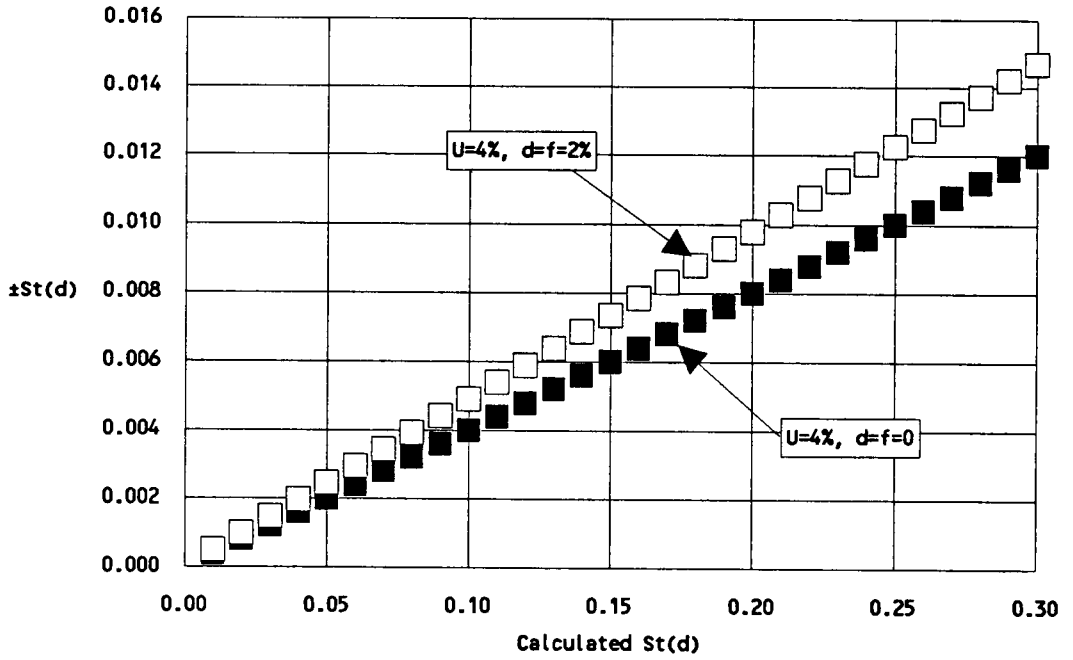

Figure 7. Estimated St number uncertainties

Table 1. Experimental water and wind tunnel St data

α	Model	REd	St(d)	St(b)	Model	REd	St(d)	St(b)
				water tunnel				
0	e=0.650	5974	0.240	0.240	b/a=0.760	5974	0.137	0.137
		9880	0.247	0.247		8634	0.121	0.121
		12175	0.249	0.249		9880	0.125	0.125
		15504	0.237	0.237		12175	0.134	0.134
	e=0.866	4000	0.253	0.253	b/a=0.500	3310	0.176	0.176
		6000	0.255	0.255		3930	0.169	0.169
		6700	0.270	0.270		4400	0.121	0.121
		7400	0.255	0.255		5680	0.093	0.093
		9800	0.260	0.260		6500	0.087	0.087
		10600	0.260	0.260		8010	0.090	0.090
		*****	*****	*****		10200	0.094	0.094
	e=0.950	2065	0.219	0.219	b/a=0.312	2452	0.178	0.178
		2452	0.230	0.230		3544	0.165	0.165
		2746	0.225	0.225		4056	0.178	0.178
		3544	0.249	0.249		5000	0.172	0.172
		3694	0.251	0.251		****	*****	*****
		4056	0.258	0.258		****	*****	*****
		5000	0.275	0.275		****	*****	*****
		5354	0.276	0.276		****	*****	*****
		6365	0.292	0.292		****	*****	*****
30	e=0.650	6492	0.219	0.202	b/a=0.760	9102	0.197	0.129
		10738	0.224	0.206		13155	0.201	0.132
		13233	0.209	0.192		15054	0.191	0.125
		16850	0.218	0.201		18551	0.203	0.133
	e=0.866	5288	0.235	0.178	b/a=0.500	6177	0.177	0.095
		7932	0.250	0.189		7333	0.217	0.116
		8857	0.248	0.188		8210	0.148	0.079
		9783	0.245	0.185		10599	0.178	0.095
		12956	0.243	0.184		12129	0.188	0.101
		14013	0.240	0.182		14947	0.199	0.107
		*****	*****	*****		19033	0.198	0.106
	e=0.950	3760	0.223	0.123	b/a=0.312	6052	0.199	0.081
		4465	0.234	0.129		8747	0.191	0.077
		4998	0.217	0.119		10010	0.204	0.083
		6453	0.189	0.104		12335	0.195	0.079
		6725	0.214	0.118		*****	*****	*****
		7384	0.250	0.137		*****	*****	*****
		9099	0.237	0.130		*****	*****	*****
		9747	0.225	0.124		*****	*****	*****
		11587	0.220	0.121		*****	*****	*****
60	e=0.650	7436	0.213	0.171	b/a=0.760	9794	0.204	0.124
		12298	0.225	0.181		14155	0.205	0.124
		15155	0.216	0.174		16198	0.201	0.125
		19298	0.217	0.174		19961	0.203	0.124

Table 1. (Continued)

α	Model	REd	St(d)	St(b)	Model	REd	St(d)	St(b)
				water tunnel				
60	e=0.866	7208	0.205	0.114	b/a=0.500	7388	0.187	0.084
		10812	0.200	0.111		8772	0.214	0.096
		12073	0.210	0.117		9821	0.153	0.069
		13335	0.200	0.111		12678	0.182	0.082
		17660	0.200	0.111		14508	0.203	0.091
		19101	0.203	0.113		17878	0.209	0.094
		*****	*****	*****		22766	0.205	0.092
	e=0.950	5826	0.181	0.064	b/a=0.312	8033	0.209	0.064
		6917	0.204	0.072		11610	0.186	0.057
		7744	0.175	0.062		13286	0.208	0.064
		9997	0.167	0.059		16372	0.209	0.064
		10419	0.186	0.066		*****	*****	*****
		11440	0.200	0.071		*****	*****	*****
		14097	0.197	0.070		*****	*****	*****
		15101	0.187	0.066		*****	*****	*****
		17952	0.201	0.071		*****	*****	*****
90	e=0.650	7860	0.219	0.166	b/a=0.760	7860	0.146	0.111
		13000	0.224	0.170		11360	0.151	0.115
		16020	0.213	0.162		13000	0.148	0.113
		20400	0.215	0.163		16020	0.149	0.113
	e=0.866	8000	0.200	0.100	b/a=0.500	6620	0.149	0.075
		12000	0.210	0.105		7860	0.174	0.088
		13400	0.200	0.100		8800	0.125	0.063
		14800	0.190	0.095		11360	0.141	0.071
		19600	0.193	0.097		13000	0.159	0.080
		21200	0.197	0.099		16020	0.168	0.084
		*****	*****	*****		20400	0.154	0.077
	e=0.950	6620	0.183	0.057	b/a=0.312	7860	0.175	0.055
		7860	0.190	0.059		11360	0.162	0.051
		8800	0.162	0.051		13000	0.172	0.054
		11360	0.177	0.055		16020	0.172	0.054
		11840	0.184	0.057		*****	*****	*****
		13000	0.194	0.061		*****	*****	*****
		16020	0.179	0.056		*****	*****	*****
		17160	0.181	0.057		*****	*****	*****
		20400	0.191	0.060		*****	*****	*****

Table 1. (Concluded)

α	Model	REd	St(d)	St(b)	Model	REd	St(d)	St(b)
				wind tunnel				
0	e=0.866	6883	0.290	0.290		*****	*****	*****
		8977	0.286	0.286		*****	*****	*****
		9907	0.282	0.282		*****	*****	*****
		9921	0.272	0.272		*****	*****	*****
		11993	0.284	0.284		*****	*****	*****
30		9099	0.242	0.183		*****	*****	*****
		11868	0.239	0.181		*****	*****	*****
		13097	0.233	0.176		*****	*****	*****
		13116	0.234	0.177		*****	*****	*****
		15855	0.234	0.177		*****	*****	*****
60		12403	0.191	0.106		*****	*****	*****
		16177	0.188	0.104		*****	*****	*****
		17852	0.193	0.107		*****	*****	*****
90		13766	0.181	0.091		*****	*****	*****
		17954	0.176	0.088		*****	*****	*****
		19814	0.182	0.091		*****	*****	*****

***** Indicates no available data

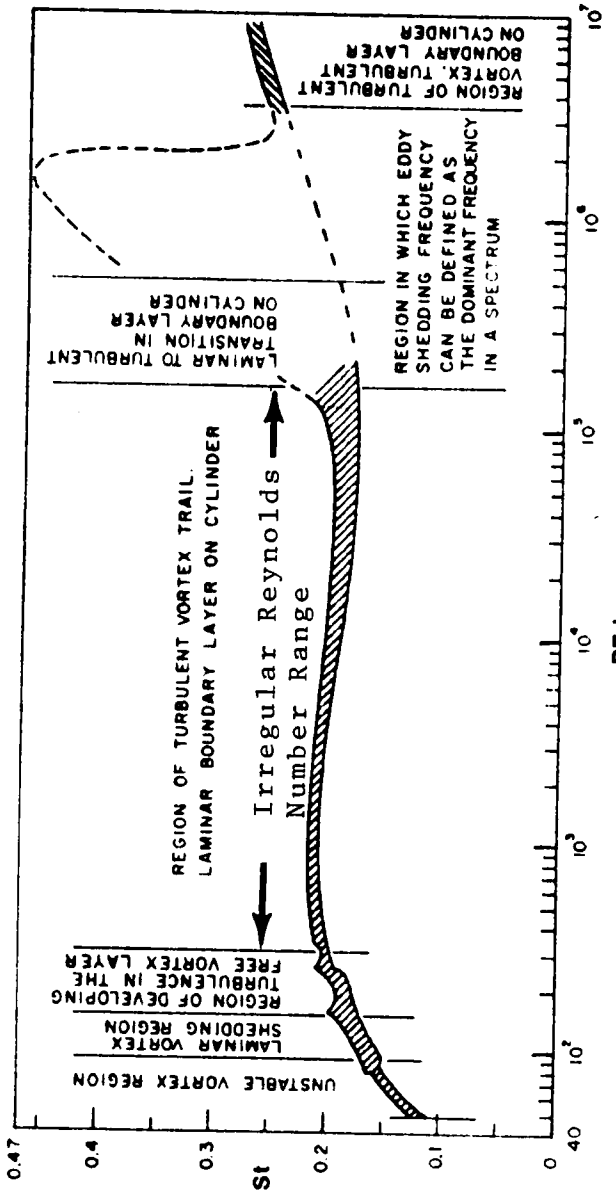

Figure 8. Strouhal-Reynolds number relationship for unyawed circular cylinders [13]

As Roshko [4] explains, the Reynolds number (REd) range 300 to 10000 is defined as the irregular range as presented in Figure 8. All of the data presented in this investigation was obtained in the irregular range and is presented in Table 1 for both the water and wind tunnel. Vortex frequency measurements were obtained approximately 2 diameters downstream behind the trailing edge (X) and 1 diameter laterally of the trailing edge (-Y) at a nominal vertical height (Z) of 6 in. as sketched in Fig. 4. All Strouhal data were corrected for tunnel blockage proposed by Tsuchiya, et al. [14]. The tunnel blockage correction factor (m) was a spinoff while developing a digital flow meter and is approximated as $m \approx 1+1.25(d/D)$ and is incorporated into the Strouhal number equation as $St=mfd/U$ for $d/D<0.35$ where D is the test section width. Documentation was found containing research at Reynolds numbers between 40 and 2000 for various body shapes with investigating different flow phenomena. For Reynolds numbers between 2000 and 10000 documentation about vortex shedding became scarce or incompatible with the current research interest. To support the current studies findings a limited amount of data from other references will be included in certain figures for comparison, but may be not be a direct comparison. Because of the limited amount of data to support the investigations findings the

introduction of an uncertainty band with the data, as discussed in Section 4.2, was warranted.

As presented in Figure 1 and 8 the Strouhal number is practically a constant value of 0.21 over the entire irregular Reynolds number range for the circular cylinder. Between the Reynolds number 40 to 300 (stable and transition range) the Strouhal number increases rapidly because of laminar vortex shedding. Fage and Johansen [9] observed the relation of the shedding frequency to the distance between the vortex layers. A free vortex layer (separated boundary layer) releases from separation points on the body. The free layer and the backflow behind the cylinder form a circulation such that fluid separates from the body at regular intervals. The distance between the vortex layers increases as the cylinder becomes more bluff and the shedding frequency decreases. In fact, the Strouhal number was defined with the distance between the free shear layers (dw) and not the body projected frontal height (d), and a new Strouhal number of approximately 0.28 was obtained for the circular cylinder and other bluff cylinder shapes in the irregular range [9]. This method of determining Strouhal number is useful in accounting for the shedding phenomena, but it requires flow visualization or other experimental techniques to determine the free layer distances as presented in Fig. 9. It also indicates that

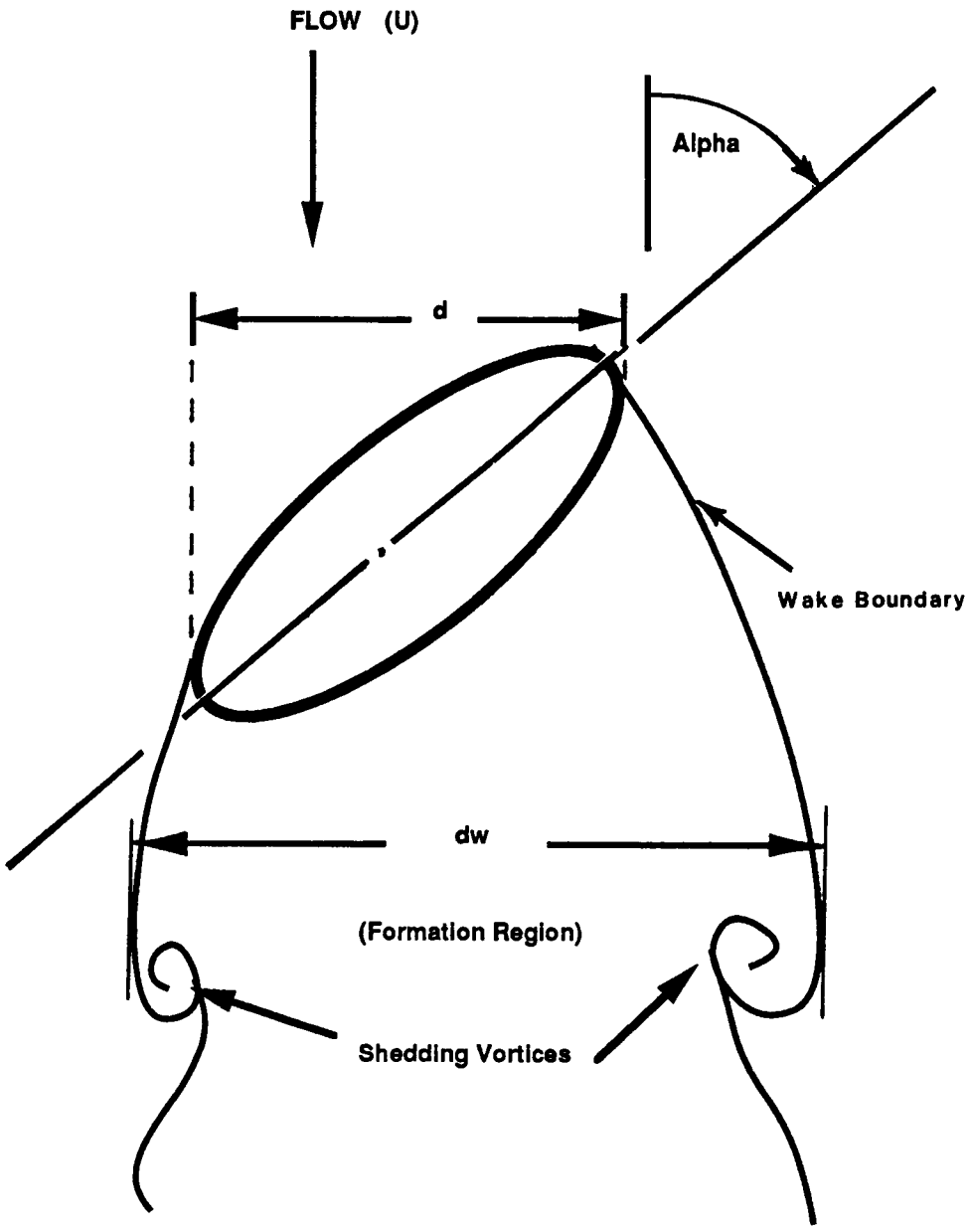

Figure 9. Formation region behind bluff bodies

when the fluid behind the body is turbulent the formation of free vortices are similar for various bluff shapes over a wide range of Reynolds numbers.

Beginning with e=0.650 the Strouhal data is presented in Fig. 10. At zero angle of attack (alpha) the Strouhal number is approximately 0.24 for Reynolds numbers between 4000 and 10000. By increasing alpha the body bluffness increases. At alpha 30, 60, and 90 deg the Strouhal number decreases to approximately 0.22. So, with an increase in bluffness the Strouhal number decreased between alpha 0 and 30 deg. The Strouhal data at 30, 60, and 90 deg are almost identical to that of a circular cylinder in the same Reynolds number range with a value of 0.21. The St values at each alpha also indicate a decrease at Red=10000 similar to that of the cylinder [5]. To compare values with previous investigations [15] data for an ellipse of e=0.625 was obtained and included in Figure 10. The data for e=0.625 was obtained at low REd with a maximum REd=1200. The exact same data for e=0.650 is presented in Figure 11 as a function of alpha for 6000<REd<20400. All data follows a smooth decreasing curve and stays within the uncertainty band. Figure 11 demonstrates a prime example between St and bluffness. As alpha increases from zero to 90 deg the cylinder bluffness increases which causes a decrease in St.

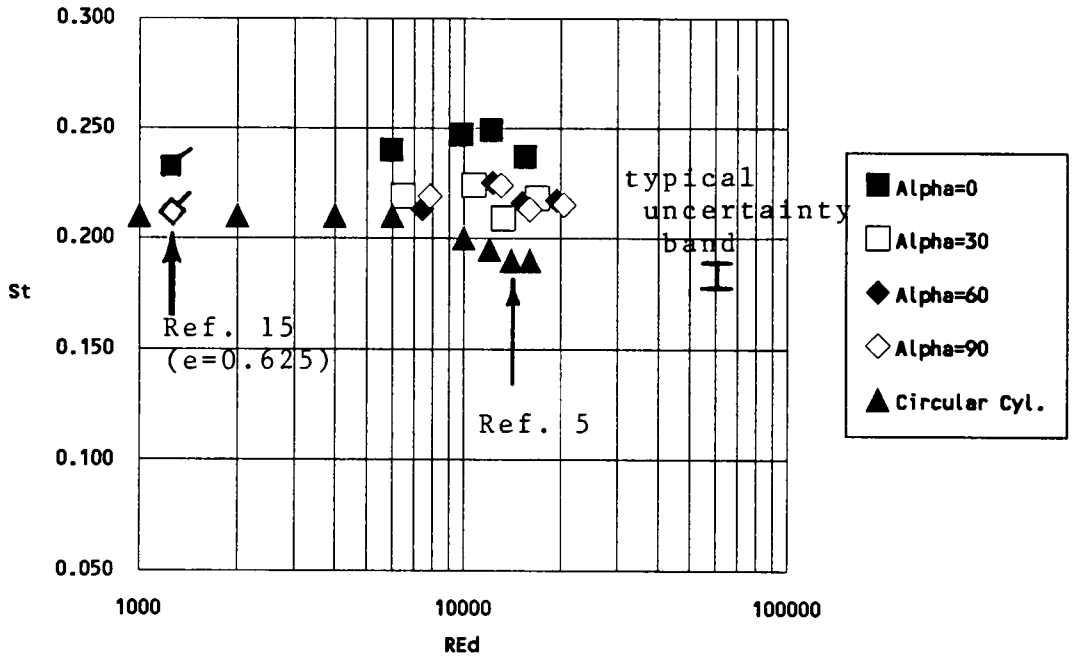

Figure 10. St variation with REd for e=0.650

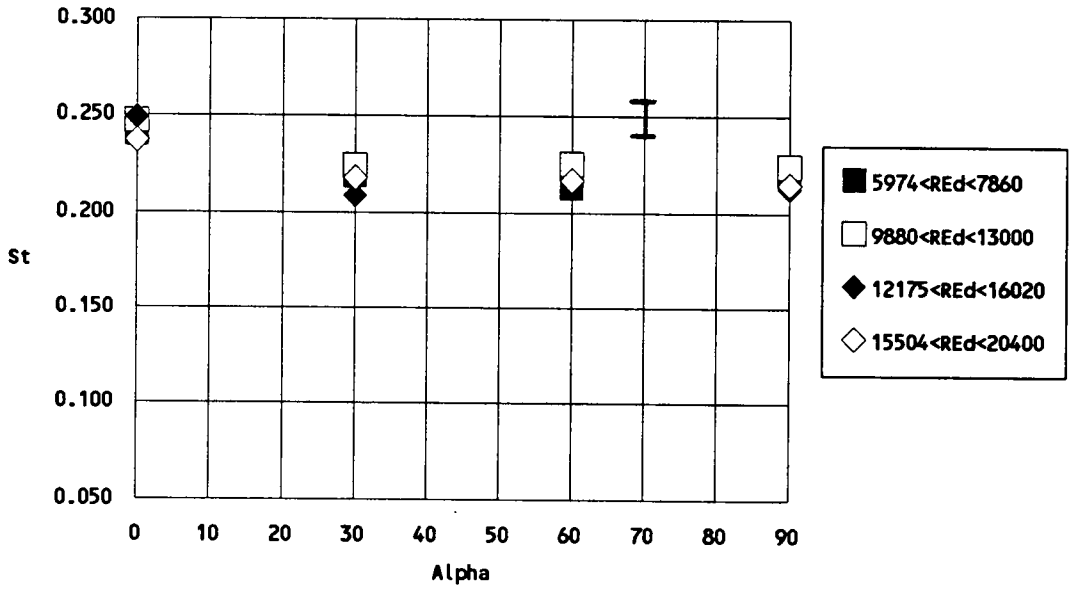

Figure 11. St variation with Alpha for e=0.650

Since the ellipse has a reduced width (b=0.760 in.) at zero alpha compared to a circular cylinder of diameter 2a (2a=1.0 in.), the flow passes the body more efficiently as discussed in Section 3.1. Again, return to Fig. 6 and note how the separation location adjusts downstream as a circular cylinder is compressed towards a thin ellipse. With the laminar separation location further downstream on the cylinder the wake width is reduced, thus Strouhal number increases to a higher value than the circular cylinder at zero alpha. Another way of explaining the increase in St is when the distance (dw) between the two separated shear layers are large (relative to vortex size), disturbances from one side take a longer time to be convected to the other side. The reverse is also true. Therefore, the vortex shedding frequency must change accordingly (i.e dw increases then f decreases). The wake region downstream of a bluff body is also critical in determining the pressure drag. Consequently, the pressure drag and Strouhal number are inversely dependent as Hoerner [16] expressed in an empirical function for two dimensional bodies as $St=0.21/Cd^n$, where n=0.75. The equation demonstrates that realistic pressure drag coefficients are the result of vortex shedding. Considering Fig. 10 and 11 in terms of Cd as the ellipse is rotated from zero alpha to 90 deg (maximum bluffness) Cd varies inversely with St.

Drag measurements or surface pressure measurements were not obtained during the study.

By continuing to compress the circular cylinder towards a thin symmetric ellipse (2a=constant) the next cylinder to be tested was of e=0.866. The Strouhal number was also a maximum value at alpha zero (Fig. 12), but a constant St value was obtained from 60 to 90 deg. The St value was 0.20 which is similar to the circular cylinder Strouhal number as presented in Figure 13. Figure 13 suggest that the bluffness for e=0.866 between 60 and 90 deg is approximately the same as the circular cylinder. For e=0.650 the similarity extended over a greater range between alpha of 30 and 60 deg. The maximum Strouhal number at zero alpha was 0.26 which was 0.02 higher than the ellipse of e=0.650. Notice also that the ellipse with e=0.866 at alpha equal to 30 deg the vortex shedding frequency was equivalent to the ellipse with e=0.650 at zero alpha. Reference data points are also presented in Fig. 12, but need further discussion.

Data from Ref. 17 indicates that no tunnel blockage correction was applied to the data. If the water tunnel blockage correction factor was omitted the Strouhal data would be reduced by approximately 0.01, thus bringing the sets of data closer to within the uncertainty band. Data from Ref. 13 was obtained from an ellipse of e=0.8

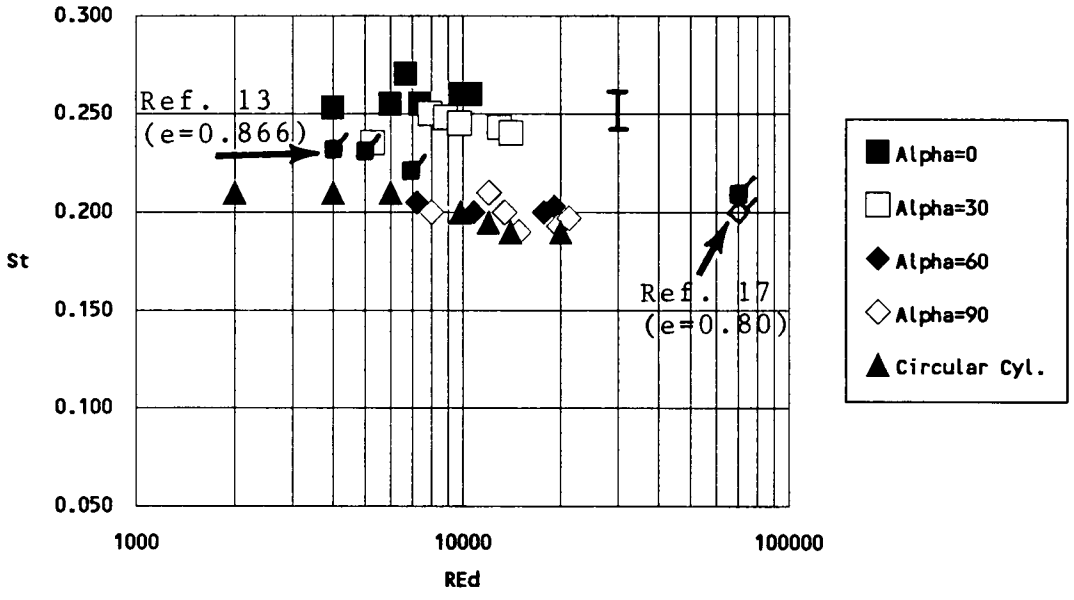

Figure 12. St variation with REd for e=0.866

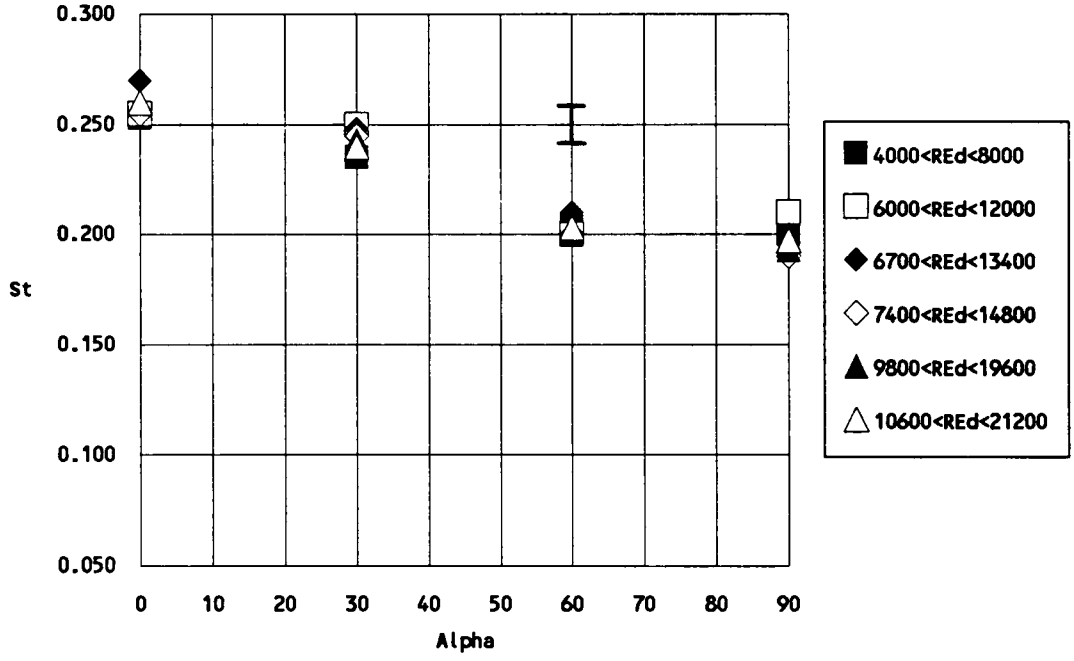

Figure 13. St variation with Alpha for e=0.866

(b/a=1.5/2.5) in a wind tunnel with the model spanning the test section. The higher Reynolds number is because of a larger model diameter required for instrumentation to measure surface pressures. No tunnel blockage correction factor was mentioned being applied. Actually, there is no significant data scatter in Ref. 14 data between e=0.6 and e=0.8 as observed in the current study. Such discrepancies in data can arise from tunnel characteristics such as tunnel freestream turbulence level differences. By increasing the tunnel turbulence level the scale of the formation region reduces, causing the shear layers to interact in a shorter time period, resulting in increased shedding frequencies [7]. Bloor [18] defines the end of the formation region as the point on the wake axis, closest to the cylinder at which a hot-wire signal, characteristic of the oscillating wake downstream, is observed. In other words, the end of the formation region is where fluid from outside the wake first crosses the cylinder axis. Fluid is drawn across the axis by the opposite strengthening vortex. Data for the ellipse with e=0.866 is presented in Fig. 12 as a function of angle of attack. To compare data trends obtained in the water tunnel for the ellipse with e=0.866 it was necessary to duplicate the trends in a different facility. The ellipse was installed in the low speed wind tunnel and tested with the results presented in Fig. 14.

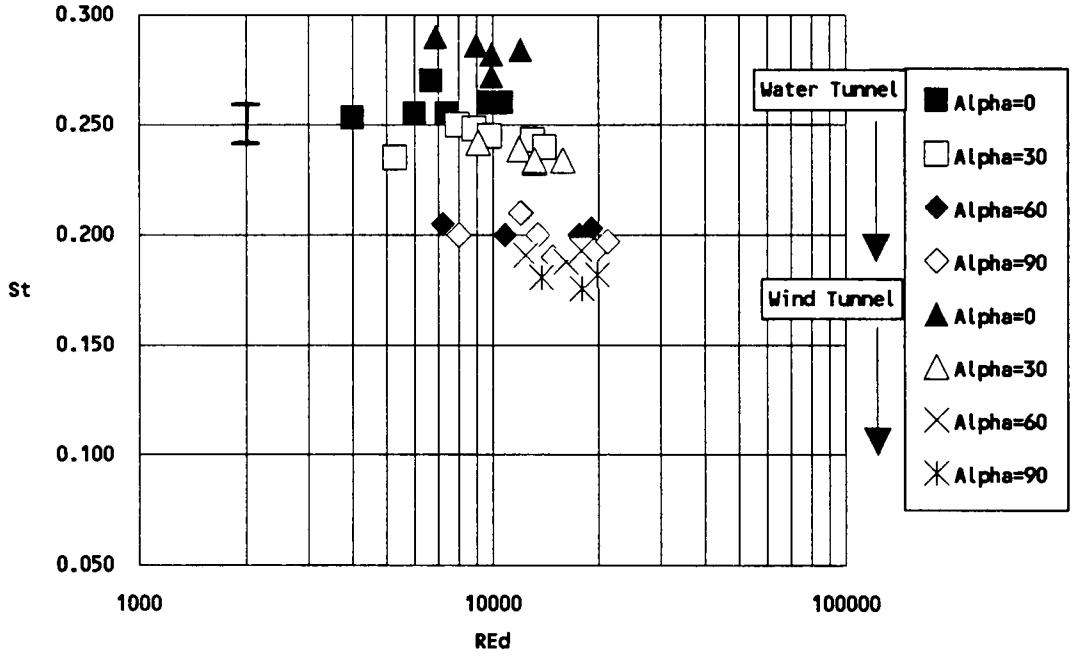

Figure 14. Water and wind tunnel St comparison for e=0.866

The zero alpha data for the wind tunnel was calculated to be approximately 0.02 higher than in the water tunnel data. An explanation could be the facilities turbulence levels and even acoustic resonance. The St data at 30, 60, and 90 deg compared within ±0.01 which was the estimated uncertainty described in Section 4.2. This result encouraged the author to continue using the water tunnel to investigate the vortex shedding frequencies for other models.

The last elliptical cylinder of highest eccentricity (e=0.950), represented a thin symmetric airfoil, indicated different vortex shedding characteristics at zero alpha than observed with the other ellipses. For zero alpha the St data increased linearly over REd from 2000 to 6500 as presented in Fig. 15. Treating the thin ellipse as a "flat plate" the boundary layer thickness (δ/x) grows along the surface $\approx 5.5/\sqrt{Re(x)}$ [5]. As the Reynolds number increases from 2000 to 6500 the boundary layer thickness reduces (i.e. δ/x=0.12 to 0.068 on both sides) with the theoretical separation point at approximately 80 percent of the surface distance as presented earlier in Fig. 6. For laminar boundary-layer flow the separation location is a function of shape only [16]. As the free shear layer separates with increasing Reynolds number the wake formation region is reduced causing an increase in vortex shedding frequency.

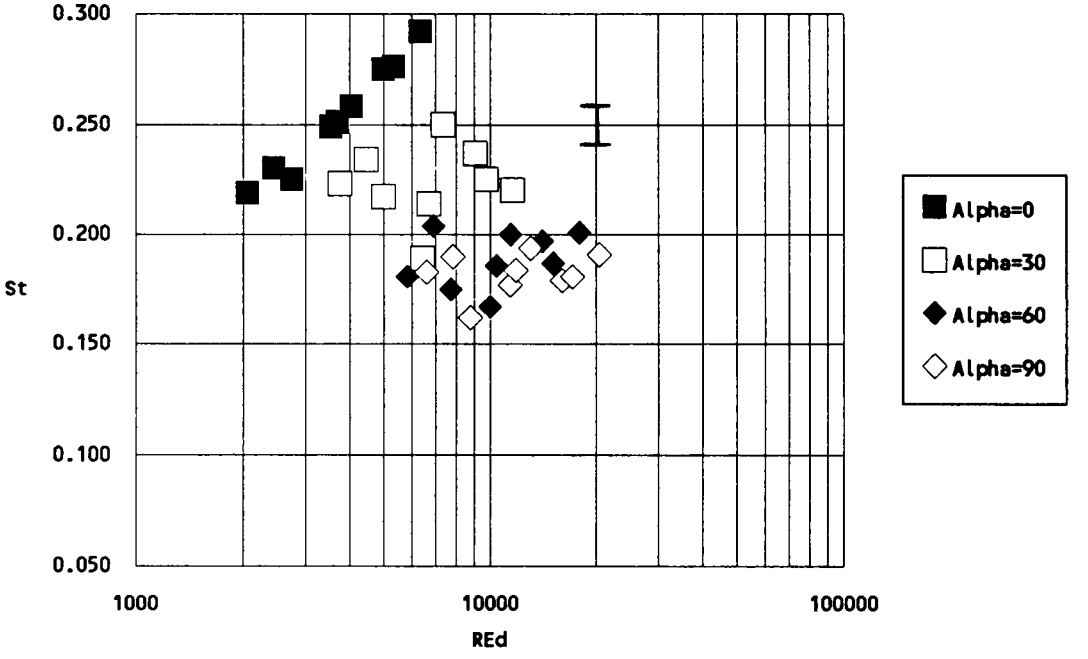

Figure 15. St variation with REd for e=0.950

The interaction of the shear layers from each side of the thin ellipse is more active in the narrow wake than the other two ellipses with larger wake region. For the first time in the irregular Reynolds number range the Strouhal number is increasing similar to the circular cylinder as presented in Fig. 1 for REd between 40 and 300 (i.e. stable range). The zero alpha St data in Fig. 15 is characteristic of laminar shedding vortices typical of the classic Karman vortex street. Photographs of the vortex street will are presented in Section 4.4. Figure 16 presents the St data for alpha over REd range 2065 to 20400. Scatter at zero alpha is because of the linear St trend in Fig. 15. The remaining St values between 30 and 90 deg alpha is experimental data scatter. To review the St data in another perspective Figs. 17 through 20 are presented for each ellipse at the same alpha.

Notice St increases linearly for e=0.950 at zero alpha in Fig. 17. The other two ellipses are approximately constant at different values of St with the ellipse of e=0.650 having the lowest St value, but still higher than the circular cylinder as referenced from Schlichting [5]. It's anticipated that the data for e=0.950 would reach a maximum St value and remain constant similar to the circular cylinder in the transition range. At 30 deg alpha in Fig. 17, the ellipse of e=0.950 has St values that

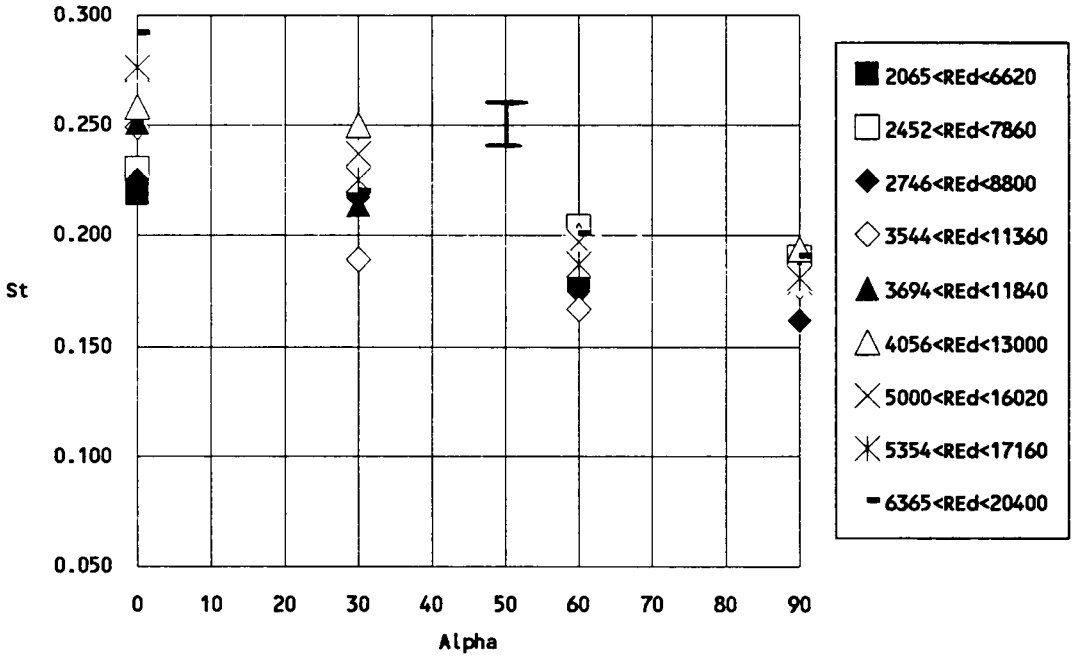

Figure 16. St variation with Alpha for e=0.950

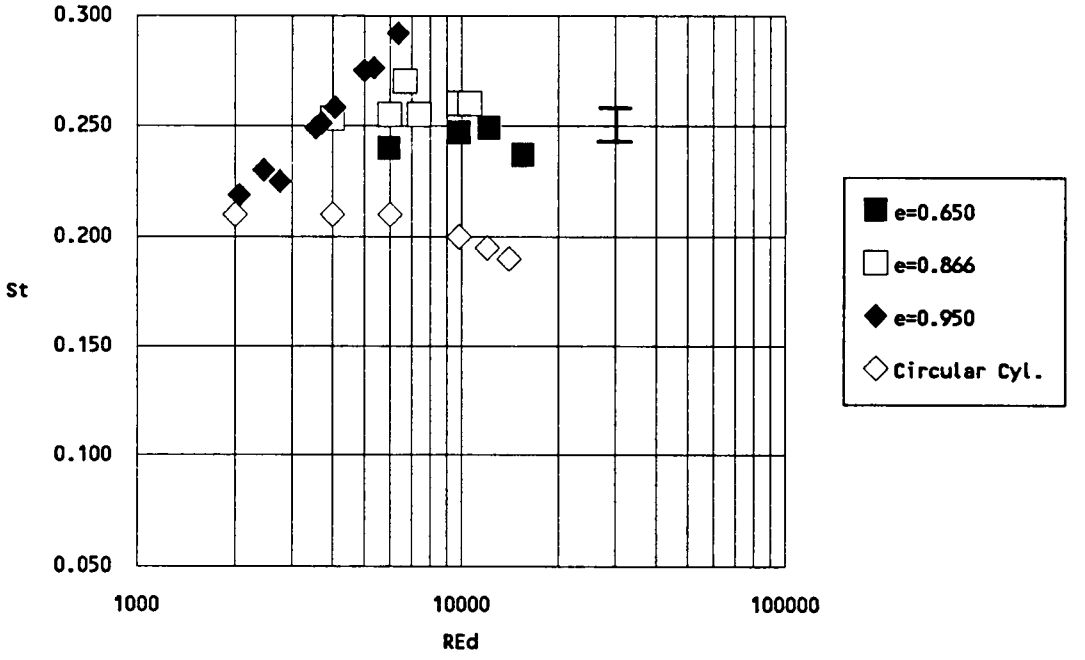

Figure 17. Comparison of St for ellipses at zero Alpha

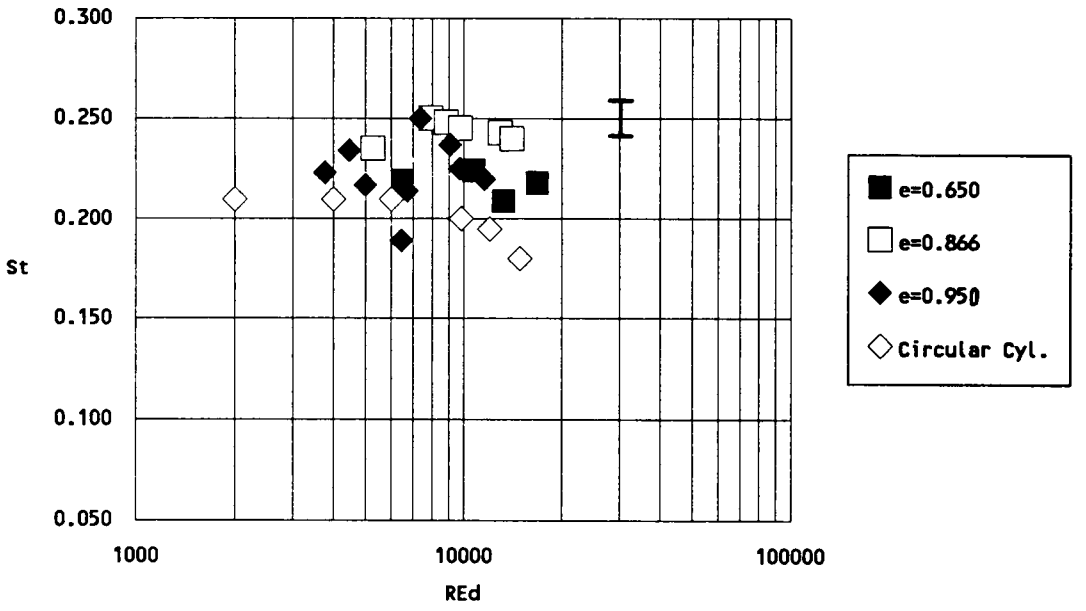

Figure 18. Comparison of St for ellipses at 30 deg Alpha

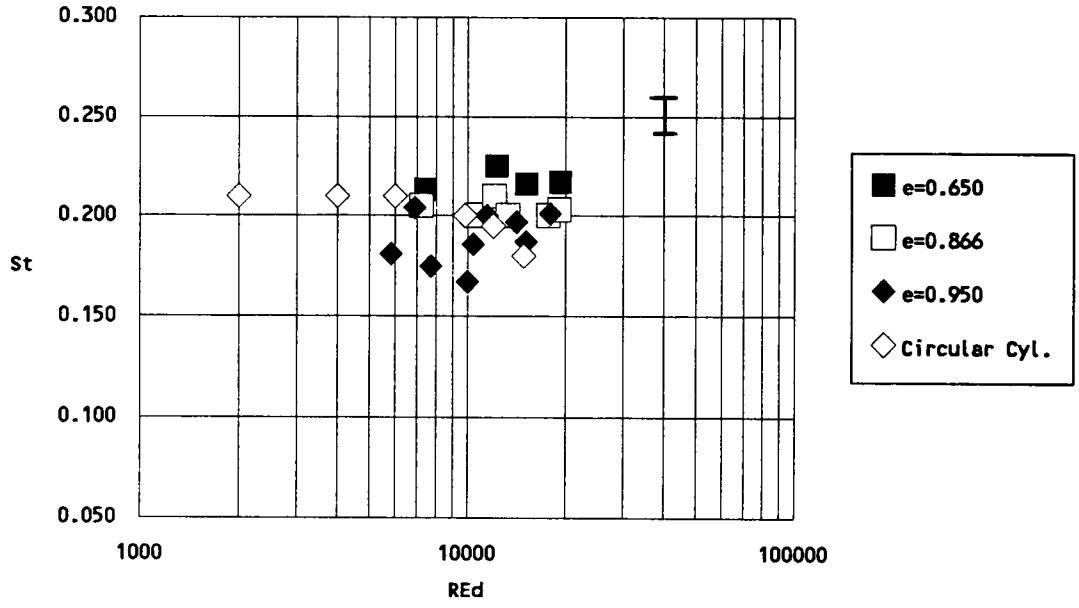

Figure 19. Comparison of St for ellipses at 60 deg Alpha

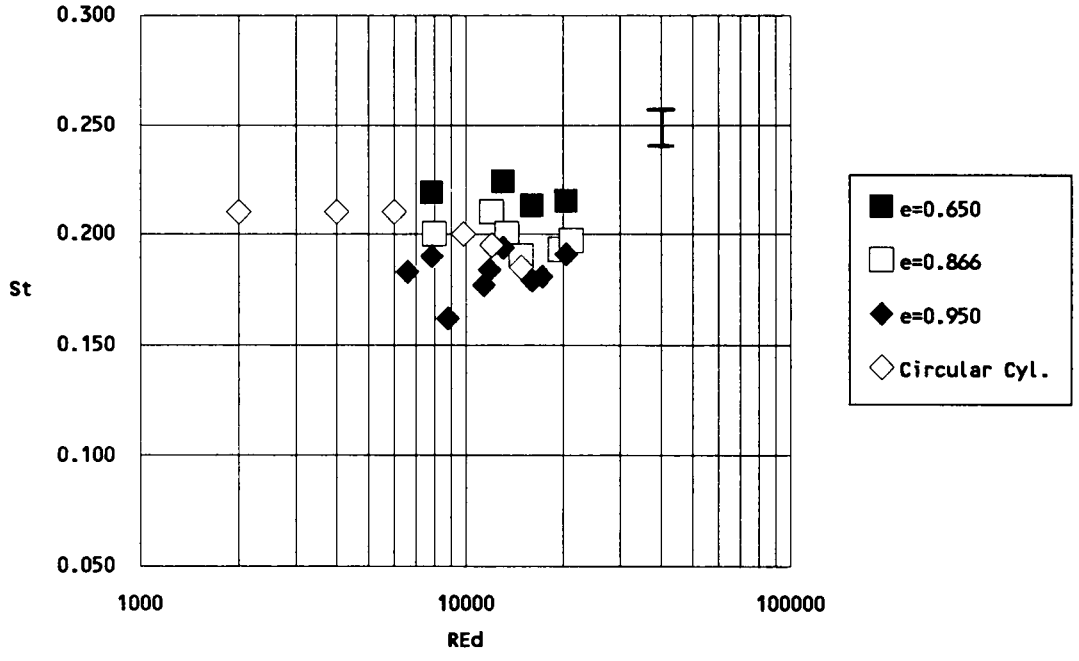

Figure 20. Comparison of St for ellipses at 90 deg Alpha

rise and fall suddenly over the entire Reynolds number range investigated making it difficult to associate a St value. It is expected that some scatter is characteristic of the data since the measurements were taken at different times, but every effort was exercised to be consistent for each test run from day to day. The application of the St estimated uncertainty for Fig. 18 is outside its intended use for e=0.950 and no constant St value can be assigned. The other two ellipses tend to follow the circular cylinder trend, but at higher relative St values. Initially, for 6000<REd<10000, St=0.175 for e=0.950 at 60 deg angle of attack (Fig. 19) and then rises to St=0.20 for REd>10000. The St value for e=0.866 is for the most part constant and equal to 0.20, but the ellipse of e=0.65 remains unchanged at St=0.22 as in previous figures. With the ellipses at their maximum bluffness of 90 deg angle of attack (Fig. 20) the ellipse of e=0.95 has the maximum bluffness resulting in the lowest Strouhal number of approximately 0.18. It's interesting to notice how the ellipses transition of bluffness changes with angle of attack resulting in reduced Strouhal numbers. At zero degrees the order of increasing bluffness was e=0.950, 0.866, and 0.650 then the circular cylinder (e=0). At 30 deg the bluffness increased in order of e=0.866, 0.650, and 0 with e=0.950 being unstable. At 60 deg the order of increasing bluffness was e=0.650,

0.866, 0.950, and 0. Finally, the order of increasing bluffness at 90 deg was e=0.650, 0.866, 0, 0.950.

Next, rectangular cylinders with smooth sides and sharp corners having fixed and stable separation points were tested. Beginning with the rectangle of width to length (b/a) ratio 0.760 the Strouhal number is presented in Fig. 21 for varying Reynolds number. Between alpha of zero and 30 deg the Strouhal number significantly increased from approximately 0.13 to 0.20 and remained constant until 60 deg where St decreased to 0.15 at 90 deg. By rotating the rectangle the leading-edge corner is directed into the flow which reduced the bluffness, thus increasing the vortex shedding frequency eventhough d is increasing. Fig. 22 presents the Strouhal data with angle of attack. Scatter in the data is within ±0.01 over the Reynolds number range 6000 to 20000. By decreasing the width of the rectangle the next model to be tested was b/a=0.500. An increase in data scatter is evident in both Figs. 23 and 24 with the Strouhal number varying between 0.09 to 0.22. With a further decrease in body width the last rectangle to be tested was b/a=0.312. As presented in Fig. 25 the Strouhal number is approximately 0.04 higher than b/a=0.760 at zero alpha because of the decrease in bluffness. Figure 26 presents data over a Reynolds number range from 2500 to 16000 with a much closer data pattern as with b/a=0.760.

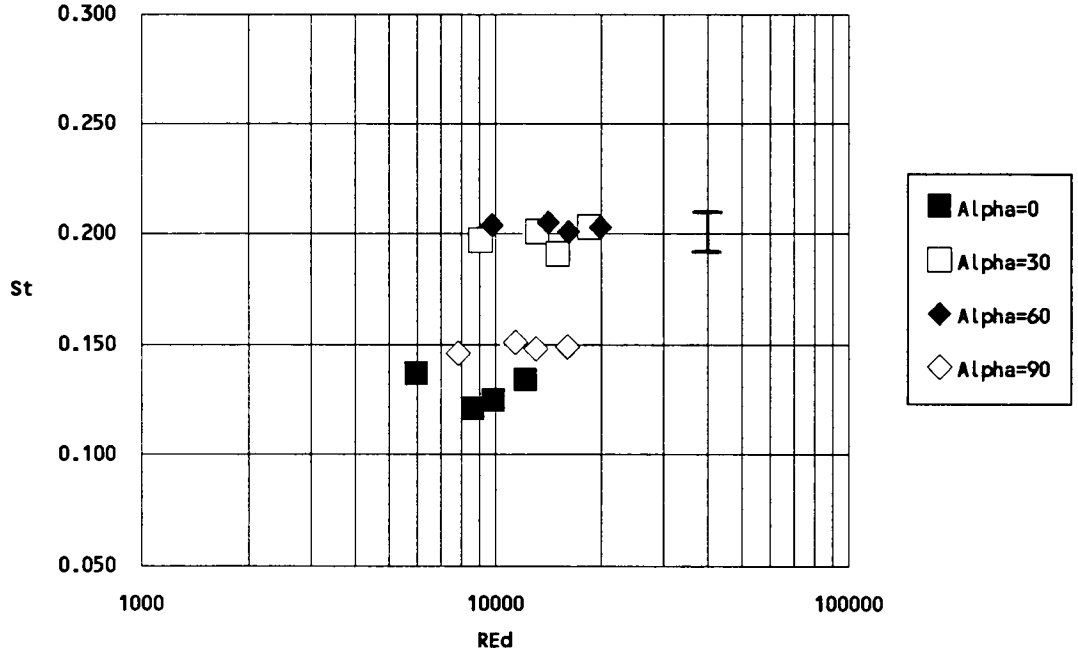

Figure 21. St variation with REd for rectangle b/a=0.760

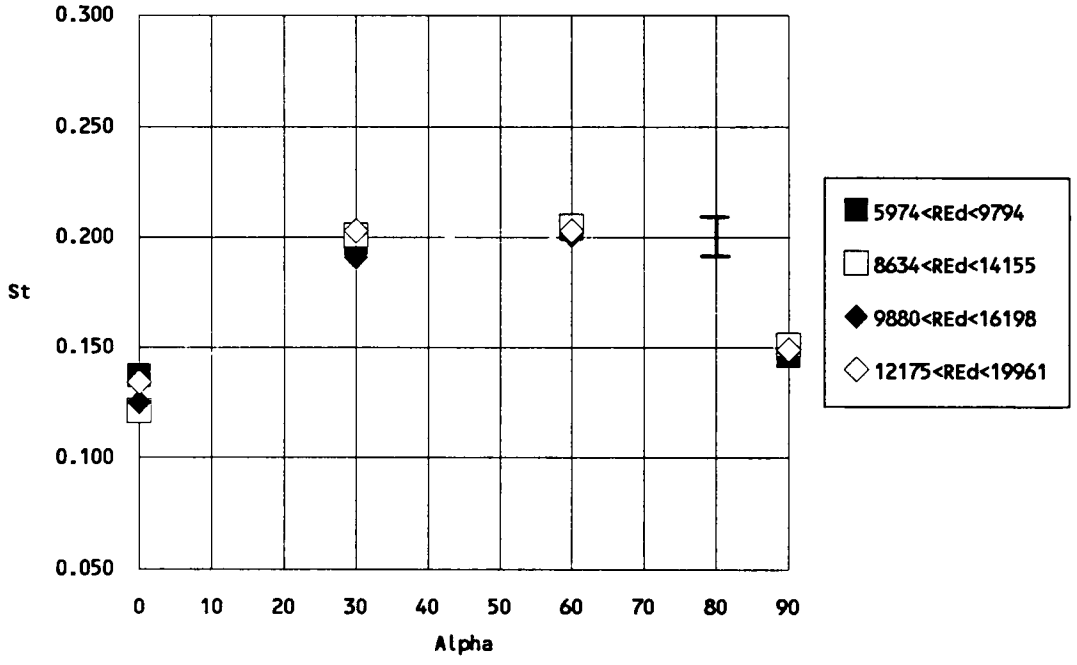

Figure 22. St variation with Alpha for rectangle b/a=0.760

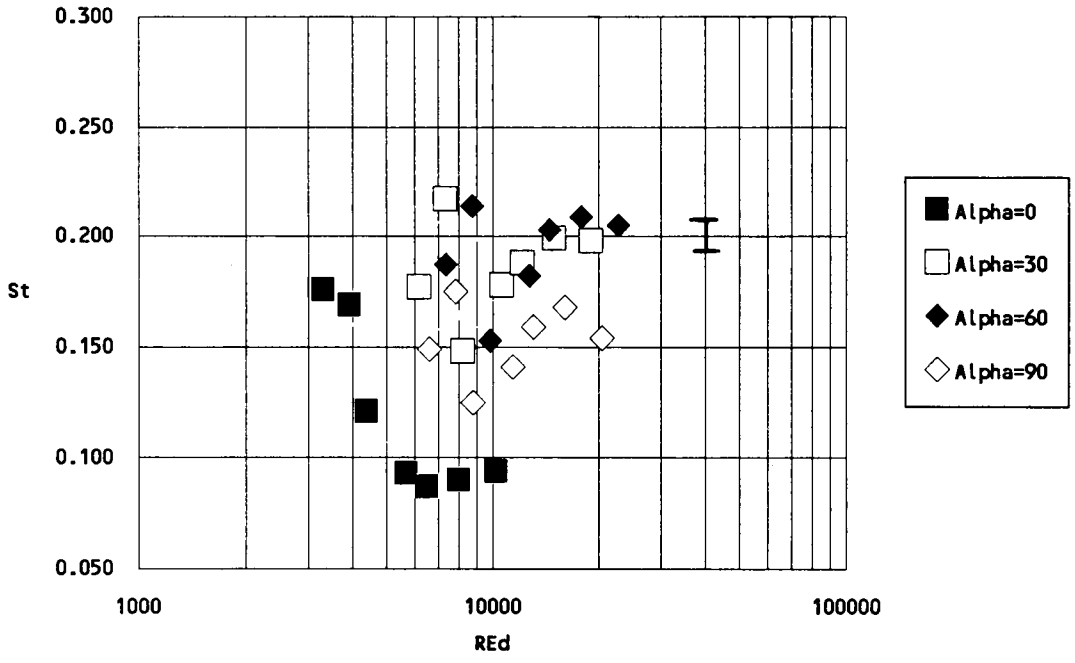

Figure 23. St variation with REd for rectangle b/a=0.500

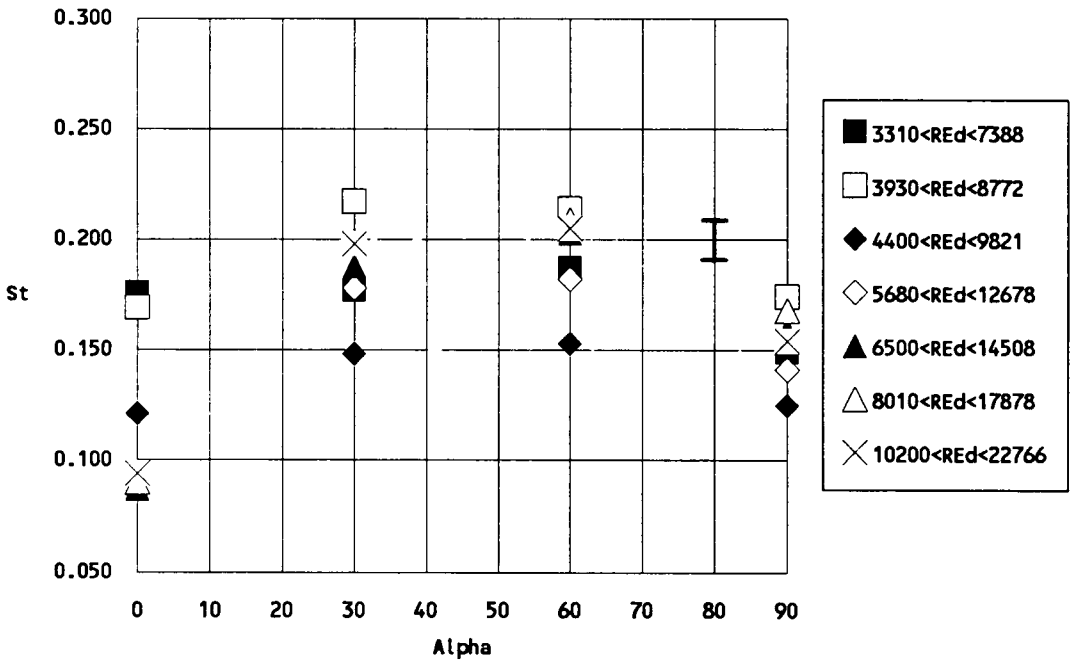

Figure 24. St variation with Alpha for rectangle b/a=0.500

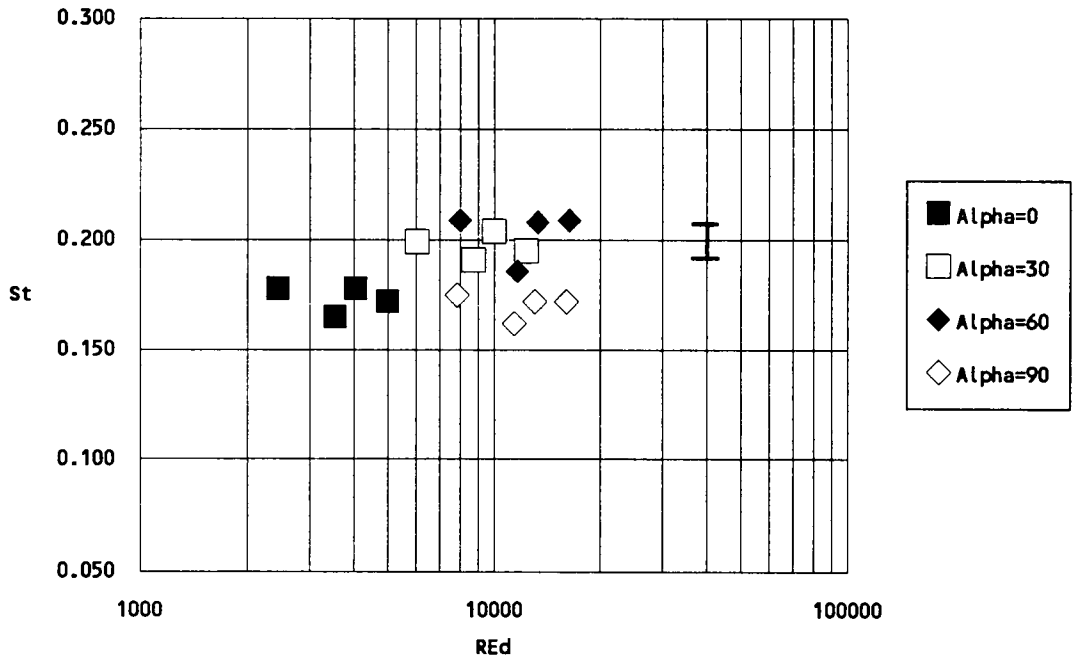

Figure 25. St variation with REd for rectangle b/a=0.312

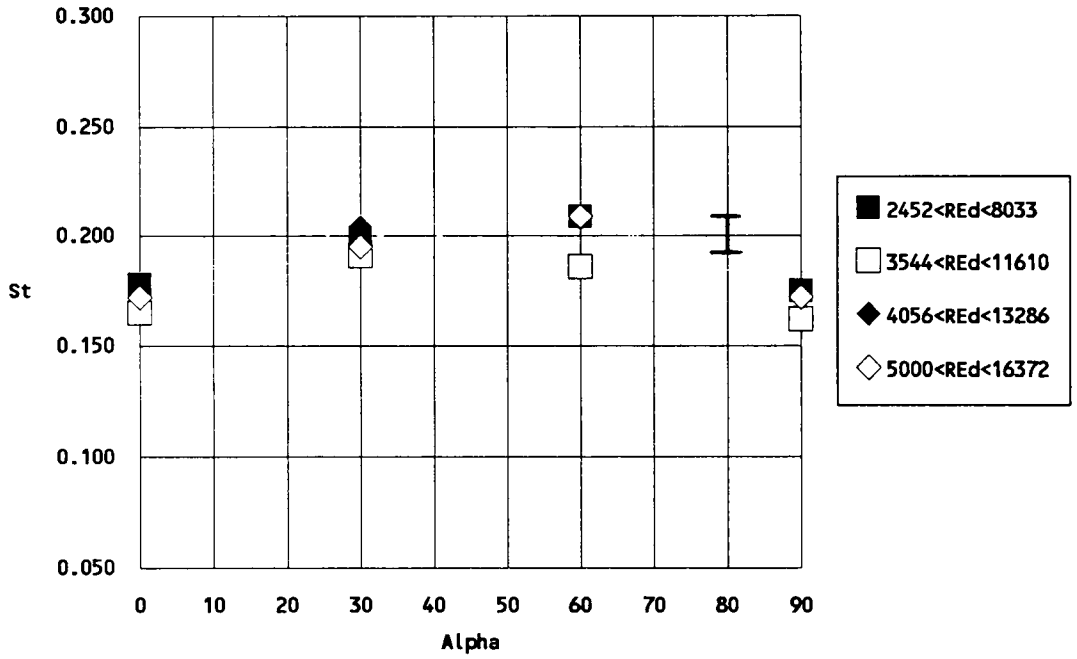

Figure 26. St variation with Alpha for rectangle b/a=0.312

As the model is rotated the Strouhal number increases to a maximum value of 0.21 at alpha of 60 deg. To present the Strouhal number data for the rectangular bodies in a different perspective Figs. 27 through 30 are useful for comparing St for different rectangles at the same angle of attack. Figure 27a represents all three rectangles at zero angle of attack over their respective Reynolds number range. As the Reynolds number increases St decreases to a minimum of 0.087 for b/a=0.500. The Strouhal number was not anticipated to be lower for b/a=0.500 than b/a=0.760 because of an decrease in d. Apparently, between b/a=0.312 and 0.760 some type of transition occurs for the rectangular cylinders causing lower vortex shedding frequencies. The transition mechanism is reattached separated flow for c/h≈2.6 [19] or b/a=0.385 as presented in Fig. 27b. It's important to note the same drop in Strouhal number for the circular cylinder referenced from Roshko [4]. With the rectangular cylinders rotated to alpha of 30 deg as presented in Fig. 28 the Strouhal number increases to a value of 0.21 which is similar to the circular cylinder. At 60 deg angle of attack the Strouhal data presented in Fig. 29 has characteristics almost identical to that in Fig. 28. At alpha of 90 deg, where all rectangular cylinders have the same d, the Strouhal number reduces to 0.16±0.01 as presented in Figure 30.

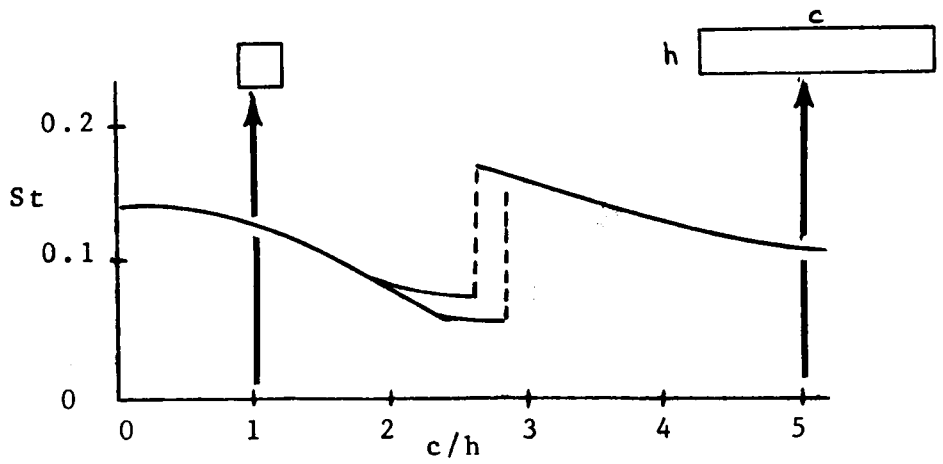

a. St transition for rectangular cylinders [19]

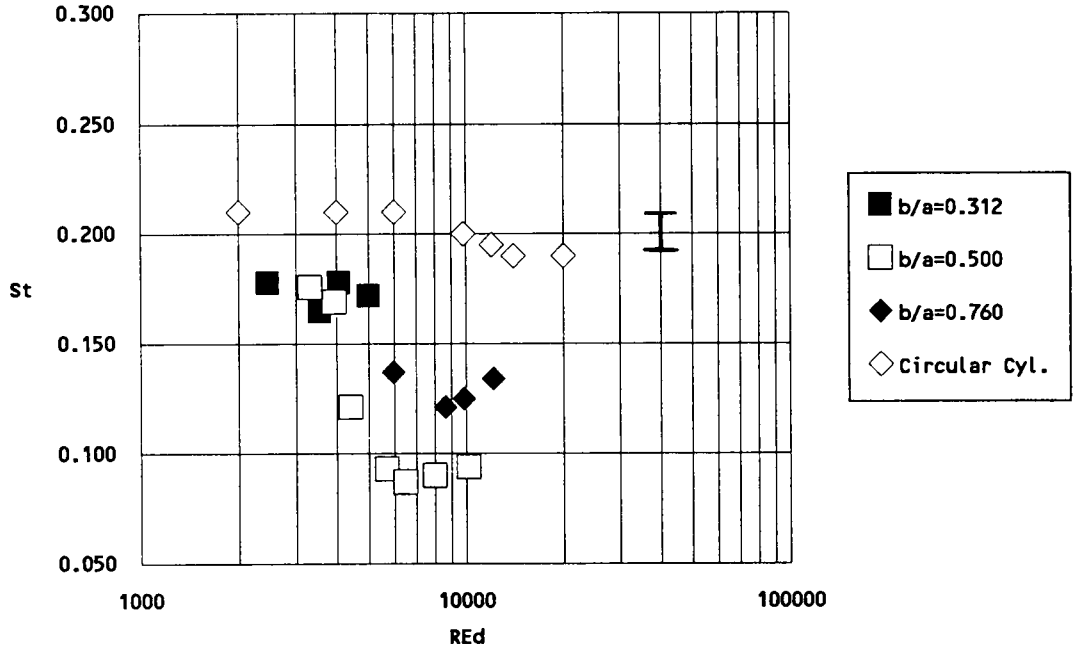

b. REd effects for rectangular cylinders

Figure 27. Comparison of St for rectangular and circular cylinders at zero Alpha

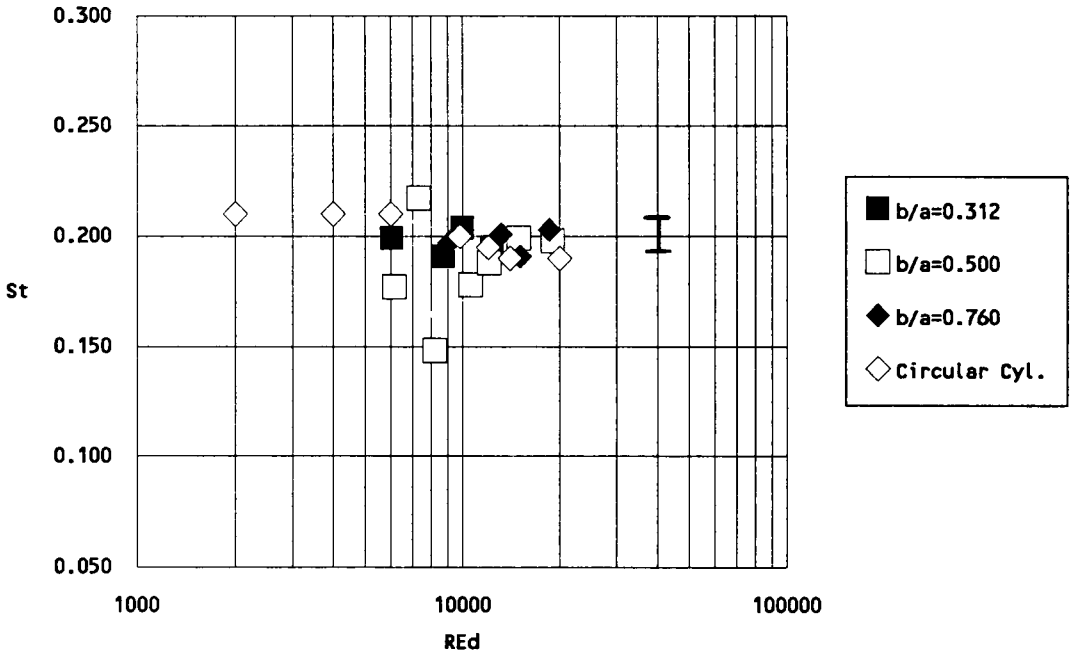

Figure 28. Comparison of St for rectangular and circular cylinders at 30 deg Alpha

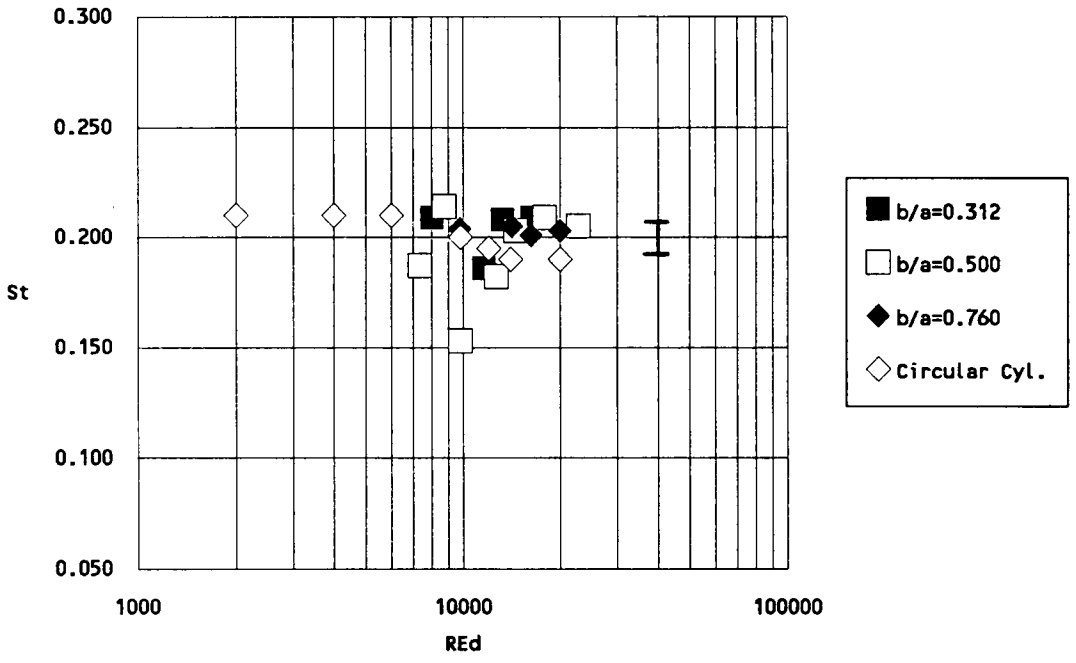

Figure 29. Comparison of St for rectangular and circular cylinders at 60 deg Alpha

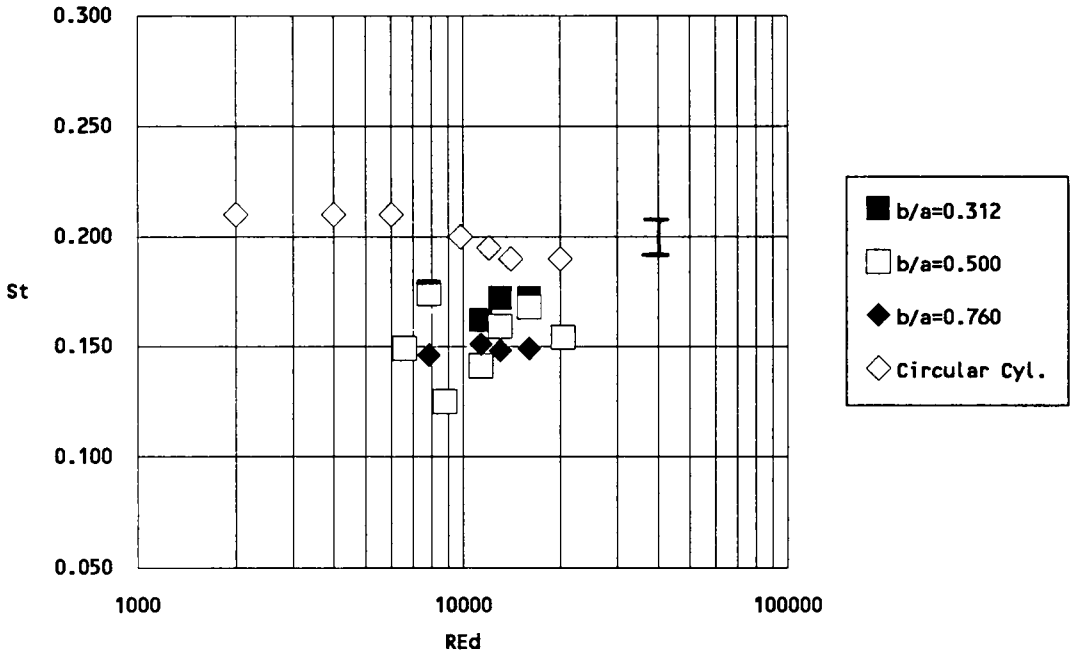

Figure 30. Comparison of St for rectangular and circular cylinders at 90 deg Alpha

Eventhough the data is within estimated uncertainty there is indication of a trend. As b/a increases at 90 deg the Strouhal number decreases. It has been argued that increasing side ratios, distance between the separation point and the position of the vortex formation, causes slightly lower shedding frequencies [12].

4.4 Universal Strouhal Number Measurements

As mentioned by Fage and Johansen [9] the Strouhal number was evaluated with the reference dimension being the distance between the free shear layers (dw) on both sides of the body in the body near wake instead of d. The new definition of Strouhal number is an attempt to define the mechanism of vortex shedding periodic disturbance (i.e. frequency). As observed by Fage and Johansen [9] the Strouhal number for a cylinder was calculated to be 0.28 using dw. By obtaining flow photographs (stills and video) the dw was extracted and used to recalculate the Strouhal numbers at the closest Reynolds number. A ruler was photographed in the water tunnel at the same location as the vortices in Fig. 31. A representative photograph of the vortex street behind the ellipse with e=0.95 and the rectangle of b/a=0.312 at zero angle of attack at Re=2233 is presented in Fig. 30. Notice that the vortex cores downstream of the ellipse, e=0.950, do not establish a

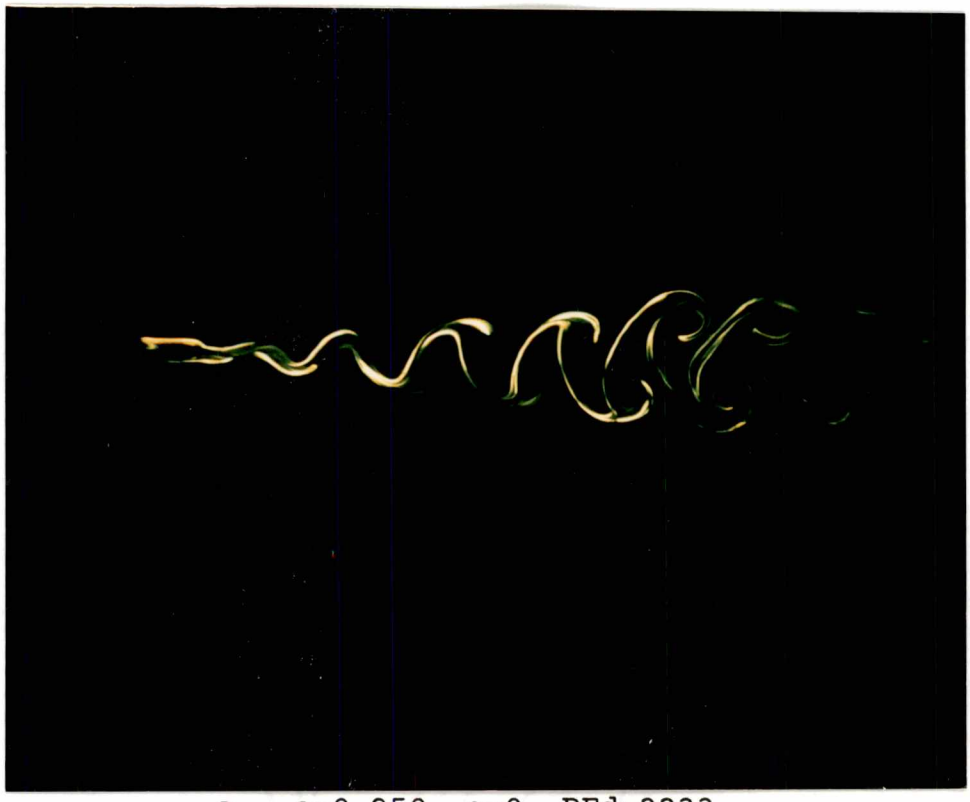

a. e=0.950, α=0, REd=2233

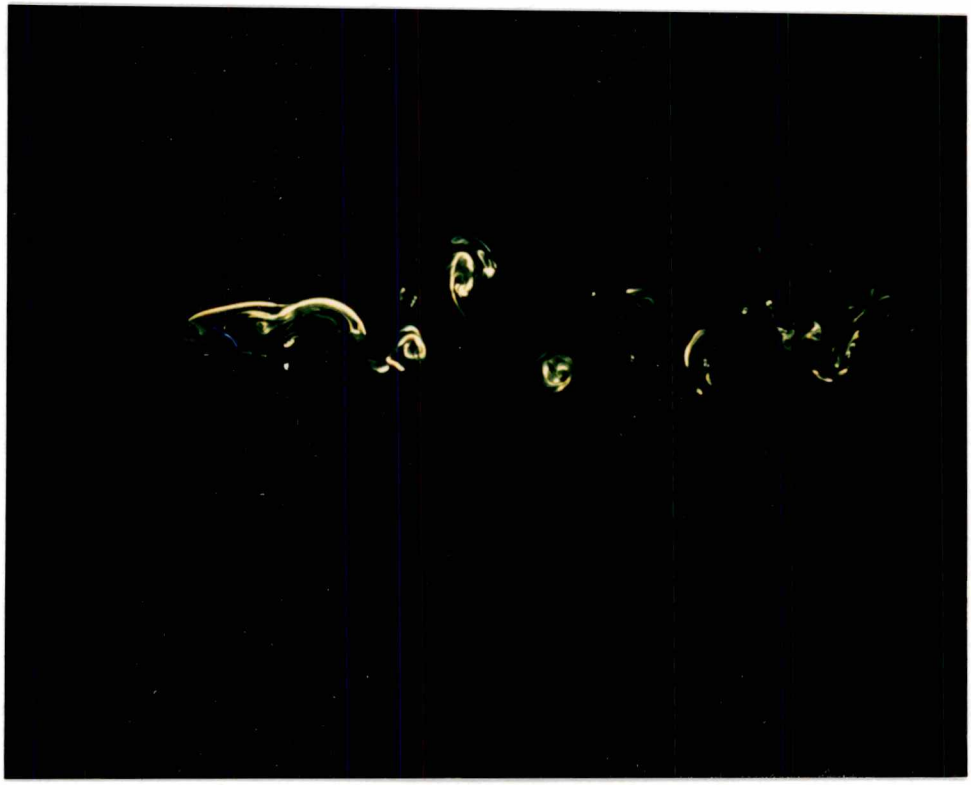

b. e=0.950, α=30, REd=4066

Figure 31. Photographs of near wake vortices

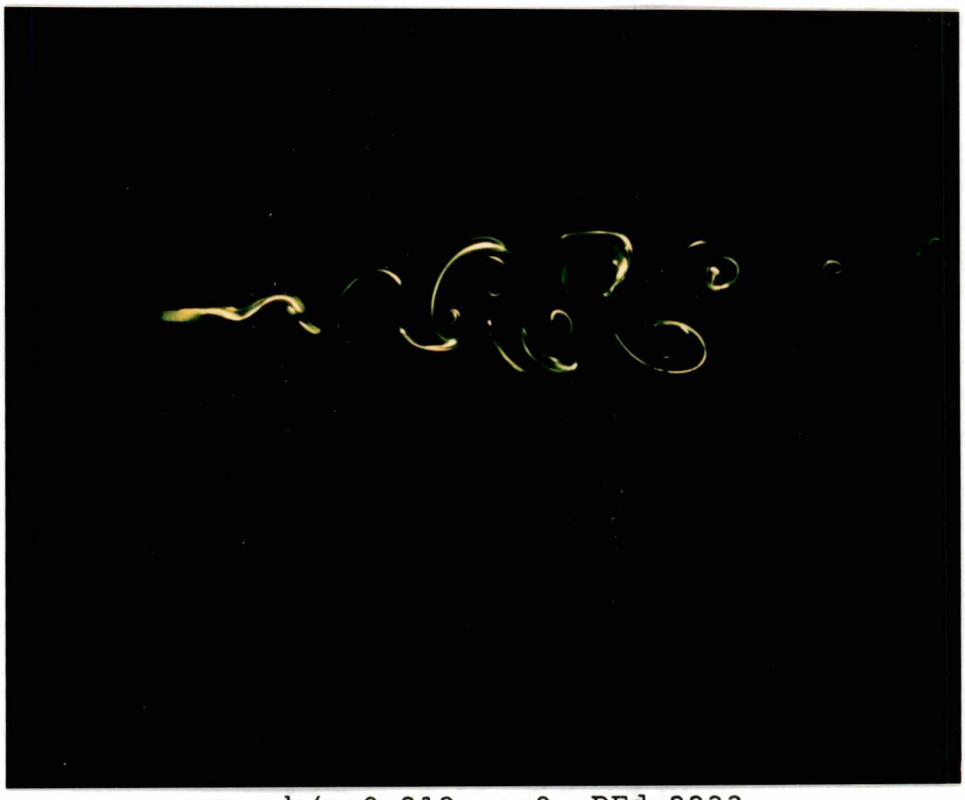

c. b/a=0.312, α=0, REd=2233



d. b/a=0.312, α=30, REd=5512
Figure 31. (Concluded)

pattern until 2 or 3 diameters. A sinusoidal wake with increasing amplitude appears in the near wake between the model trailing edge and the first established vortex core. This alternating pattern is characteristic of the classical Karman streets produced by a circular cylinder in the stable Red range (40<REd<150), but at a higher Red. As presented in Fig. 32 the scatter in the St data is reduced by a factor of 3 when dw was used instead of d. Also, the approximate St' value for all three ellipses (e=0.650, 0.866, and 0.950) at 0, 30, 60, and 90 deg angle of attack was determined to be 0.30 for 2200<REd<7200. For the rectangular bodies the same method of measuring dw was used, but reducing the St data to a common value was unsuccessful.

Finally, the dw values used to collapse the St data in Fig. 32 were normalized by d and presented in Fig.33. Notice that the upper curve is representative of maximum bluffness starting with a circular cylinder [9] and approaching a flat plate (i.e. e=1). Depending on alpha and the eccentricity of smooth cylinders there are various number of paths to follow determining the near wake shear layer distance dw. Again, notice as the body becomes bluffer dw/d increases. The use of the distance between near wake shear layers was successful for elliptical cylinders in obtaining St'. The tabulated data is

presented in Table 2 for all elliptical and rectangular models.

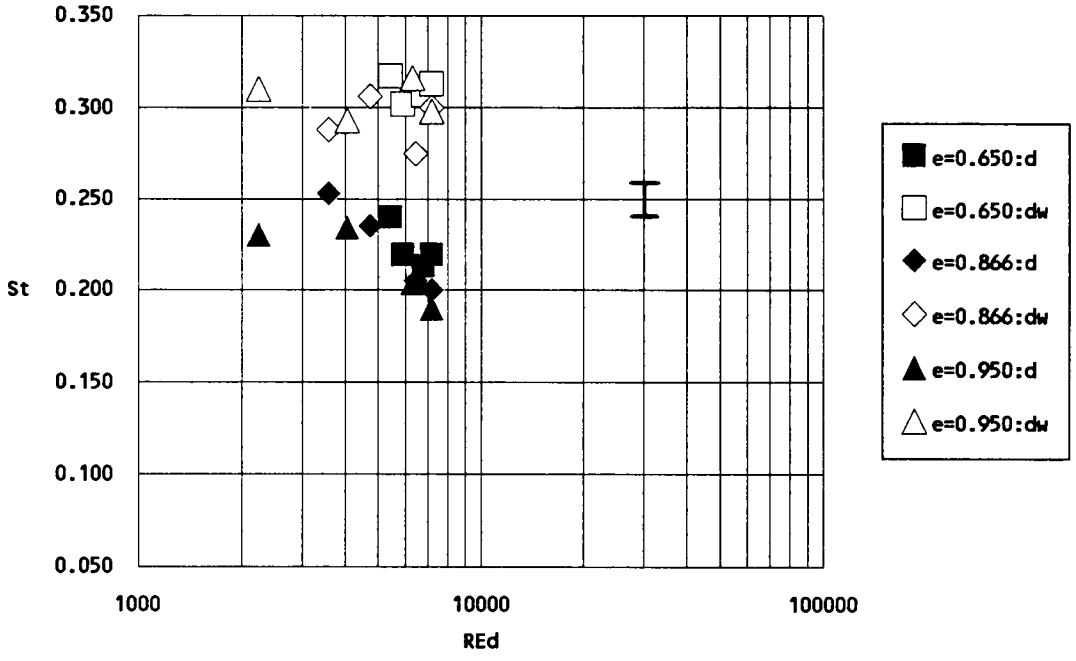

Figure 32. St based on d and dw for elliptical cylinders

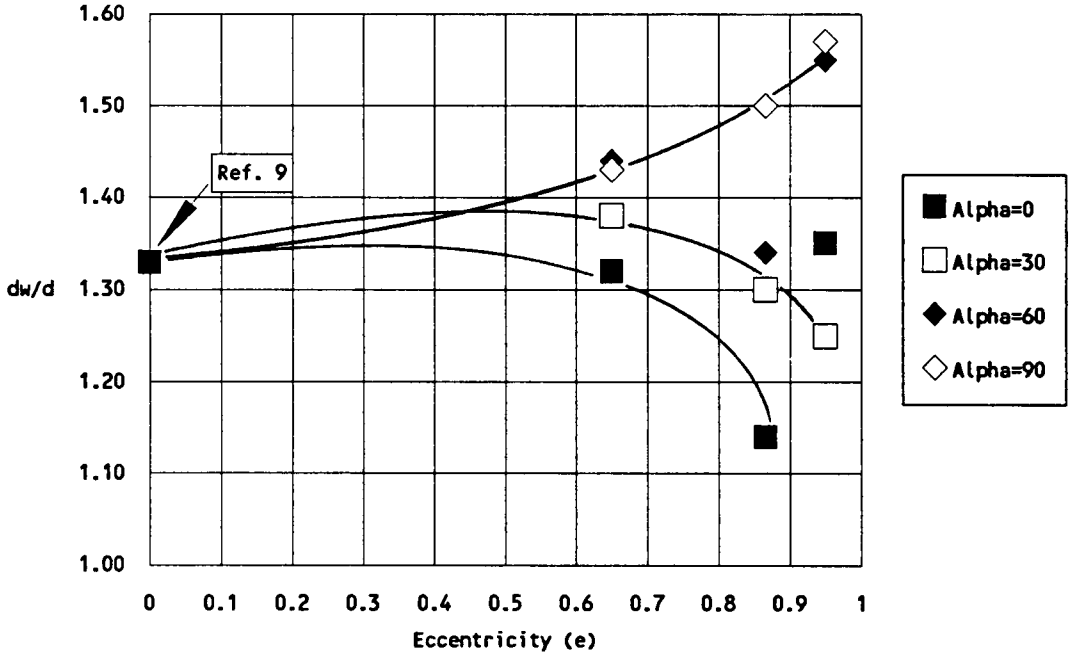

Figure 33. Variation of dw/d with e from 0 to 90 deg Alpha

Table 2. Experimental calculation of St based on dw

Model	REd (Table 1)	REd (Photo)	St	St'	α	dw	dw/d
e=0.950	2452	2233	0.230	0.310	0	0.420	1.350
	4465	4066	0.234	0.293	30	0.710	1.250
	6917	6300	0.204	0.316	60	1.360	1.550
	7860	7158	0.190	0.298	90	1.570	1.570
e=0.866	4000	3580	0.253	0.288	0	0.570	1.140
	5288	4732	0.235	0.306	30	0.860	1.300
	7208	6450	0.205	0.275	60	1.210	1.340
	8000	7158	0.200	0.300	90	1.500	1.500
e=0.650	5974	5440	0.240	0.317	0	1.000	1.320
	6492	5913	0.219	0.302	30	1.140	1.380
	7436	6772	0.213	0.307	60	1.360	1.440
	7860	7158	0.219	0.313	90	1.430	1.430
b/a=0.312	2452	2233	0.178	0.205	0	0.360	1.150
	6052	5512	0.199	0.249	30	0.960	1.250
	8033	7316	0.209	0.320	60	1.570	1.540
	7860	7158	0.175	0.299	90	1.710	1.710
b/a=0.500	3930	3580	0.169	0.240	0	0.710	1.420
	7333	6679	0.217	0.349	30	1.500	1.610
	8772	7989	0.214	0.327	60	1.710	1.530
	7860	7158	0.175	0.326	90	1.860	1.860
b/a=0.760	5974	5440	0.137	0.258	0	1.430	1.880
	9102	8289	0.197	0.317	30	1.860	1.610
	9794	8919	0.204	0.279	60	1.710	1.370
	7860	7158	0.146	0.260	90	1.780	1.780

V. GEOMETRIC INTERPRETATION OF STROUHAL NUMBER

It is interesting to note that if the Strouhal number reference length is held constant rather than varying with alpha the trend is different for both the ellipse and rectangle. As presented in Fig. 34 the solid symbols are St data calculated using the varying cylinder projection, d, and the open symbols are calculated using the minor axes dimension of the ellipse (zero alpha d=b). As mentioned, when the body is rotated the bluffness increases and shedding frequency decreases. So, the projected dimension d is changing at a positive rate in an attempt to maintain a constant St. Figure 35 presents the increasing change of d with alpha. For the rectangular cylinders the St curve has an arch shape when St is calculated with d and basically remains constant and flat based on b as presented in Fig. 36. The arch shape in St for varying alpha is directly related to the projected dimension d with alpha in Fig. 37. For the rectangular cylinders the change in St is being driven by d rather than the shedding frequency (f). This suggests that the shedding vortices have essentially the same shedding frequency at any angle of attack.

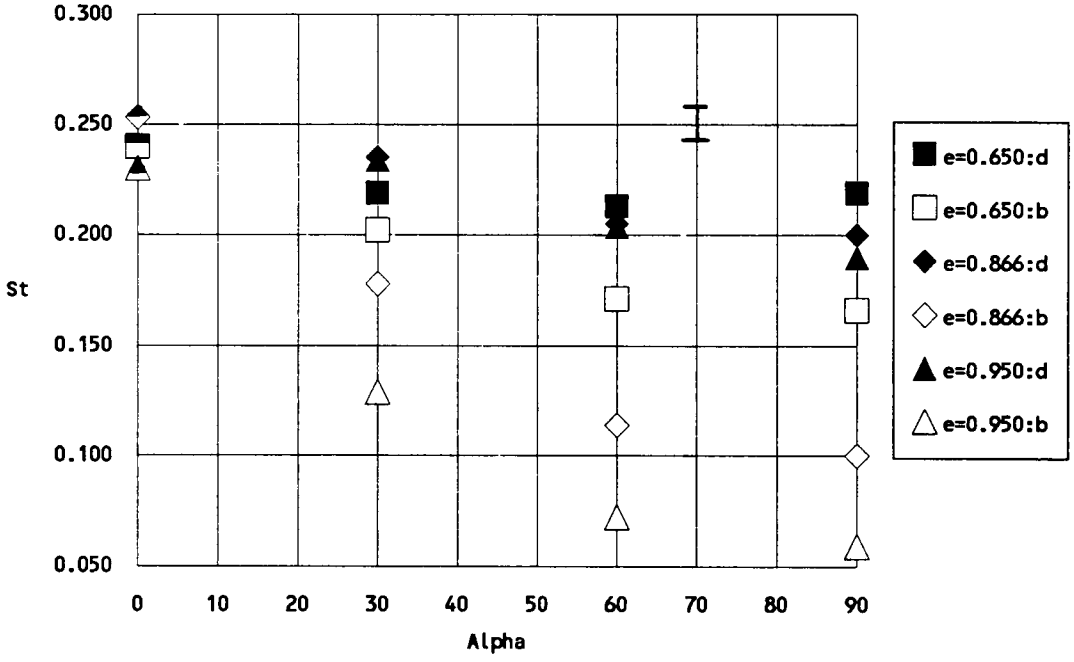

Figure 34. St based on d and b for the ellipses

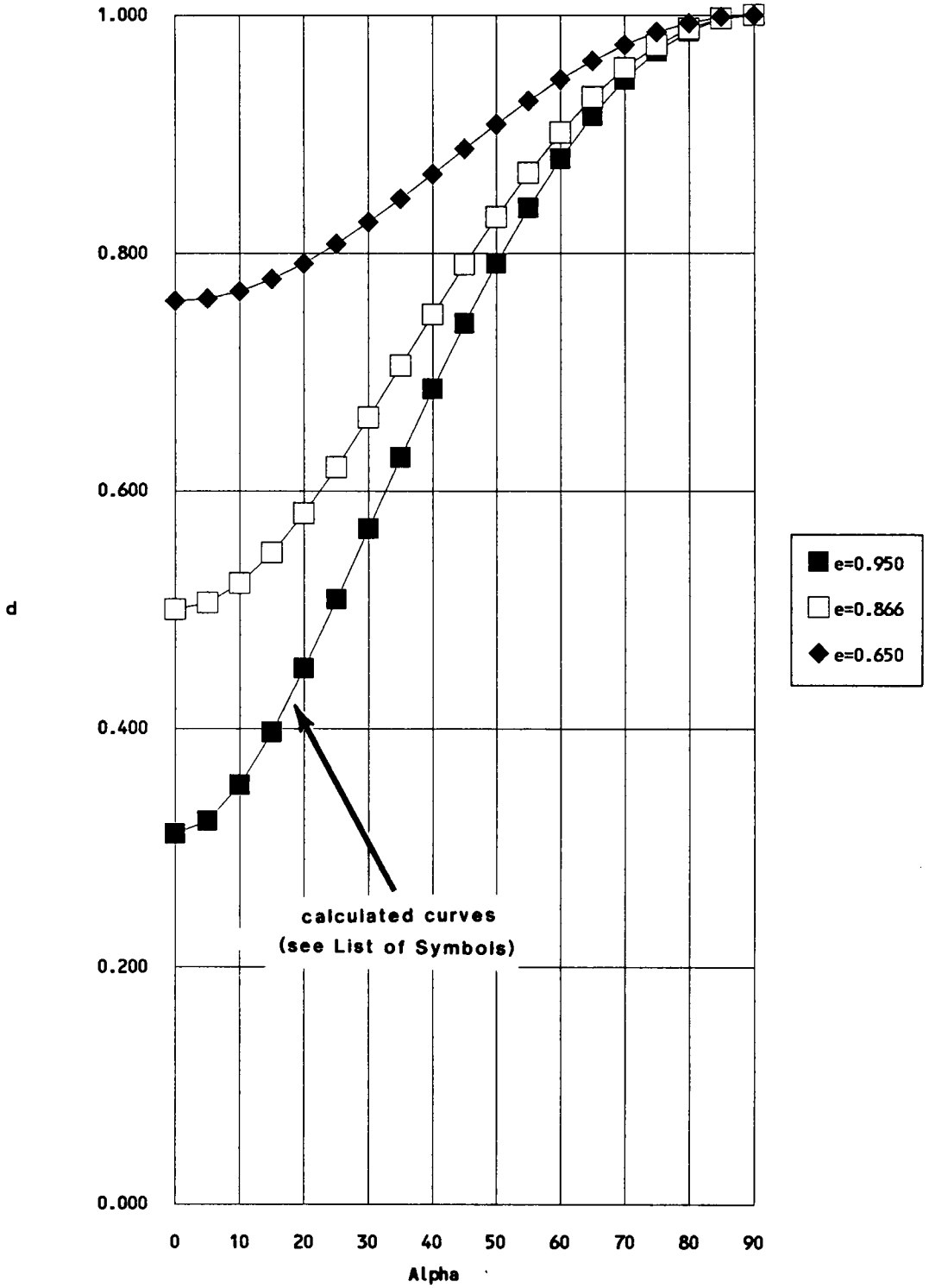

Figure 35. Variation of d with Alpha for the ellipses

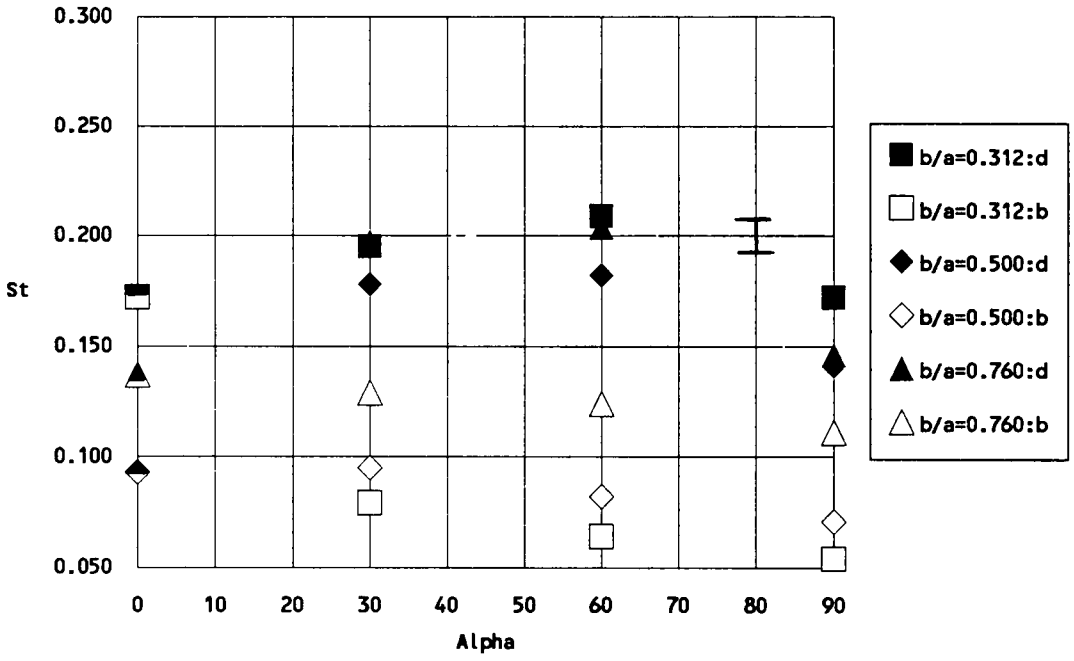

Figure 36. St based on d and b for the rectangles

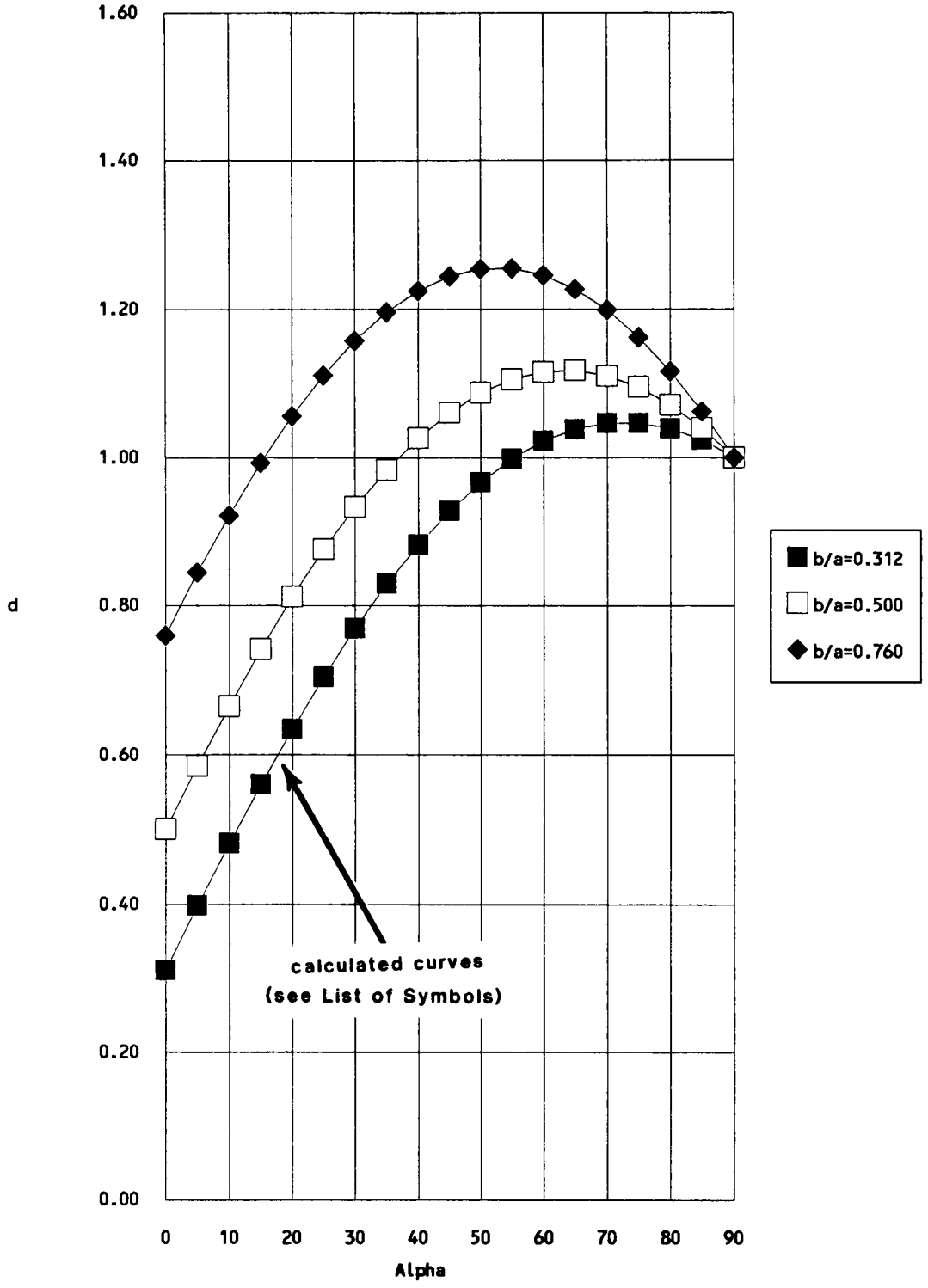

Figure 37. Variation of d with Alpha for the rectangles

VI. CONCLUSIONS

An experimental study of near wake vortex shedding characteristics behind elliptical and rectangular cylinders were analyzed in terms of the Strouhal number (St) and compared to the classic Strouhal-Reynolds number curve for circular cylinders. The test models consisted of smooth surface elliptical models with eccentricity values 0.650, 0.866, 0.950 and sharp corner rectangular cylinders with width-to-length ratios (b/a) 0.760, 0.500, and 0.312. The Reynolds number (REd) range varied from approximately 2000 to 23000, defined as the irregular range, for model angles of attack relative to the freestream flow of 0, 30, 60, and 90 deg. The conclusions of the study are listed below as follows:

1. Discrepancies in obtaining test section freestream velocity were minimized by applying Roshkos'[4] nondimensional shedding frequency (F) method in the irregular Reynolds number range.
2. The Strouhal number, based on d and b, decreased with increasing bluffness for the ellipses with eccentricity (e) 0.650, 0.866, and 0.950 with the maximum Strouhal number at zero alpha.
3. The Strouhal number, based on d, reached maximum values between 30 and 60 deg for rectangular cylinders for width to length (b/a) ratios 0.760, 0.500, and 0.312.

4. The use of d and b for rectangular cylinders caused St to have entirely different characteristics indicating careful selection of a reference dimension is required for meaningful representation.

5. The ellipse of e=0.950 at zero alpha produced increasing vortex shedding frequencies over 2000<REd<6300 resulting in linearly increasing St values ranging from 0.22 to 0.29. The trend had similar characteristics of the laminar Karman vortex streets produced by a circular cylinder for 40<REd<150.

6. The vortex formation region reference distance (dw) was successfully used in obtaining a universal Strouhal number of 0.30 for the elliptical cylinders over 2400<REd<8000 for alpha between zero and 90 deg, but was unsuccessful for the rectangular cylinders.

7. A relation between dw/d, e, and alpha was graphically constructed from data that was used to collapse the elliptical cylinders Strouhal number to a universal Strouhal number of 0.30. Efforts to determine a single empirical equation containing dw/d, e, and alpha may exist, but could not be determined.

LIST OF REFERENCES

LIST OF REFERENCES

1. Strouhal, V., "Uber eine besondere Art der Tonerregung," Ann. Phys. und Chemie, Neue Folge, Bd. 5, Heft 10, pp. 216-251, October 1878.

2. Ahlborn, F., "Uber den Mechanismus des Hydro-dynamischen Widerstandes," Abh. Geb. Naturwiss., Bd. 17, 1902.

3. Von Karman, Th., and Rubach, H., "Uber den Mechanismus des Flussigkeits und Luftwiderstandes," Phys. Zs., Bd. 13, Heft 2, pp. 49-59, January 15 1912.

4. Roshko, A., "On the Development of Turbulent Wakes from Vortex Streets," NACA Report 1191, 1954.

5. Schlichting, Dr. Hermann, Boundary Layer Theory, McGray-Hill, Seventh Edition, 1955.

6. Roshko, A., "On the Drag and Shedding Frequency of Two-Dimensional Bluff Bodies," NACA TN 3169, July 1954.

7. Gerrard, J.H., "The Mechanics of the Formation Region of Vortices behind Bluff Bodies," Journal of Fluid Mechanics, Vol. 25, part 2, pp. 401-413, June 1966.

8. Bearman, P.W., "On Vortex Street Wakes," Journal of Fluid Mechanics, Vol. 28, pp.625-641, 1967.

9. Fage, A., and Johansen, F.C., "The Structure of Vortex Sheets, "R&M, No. 1143, British A.R.C., 1927.

10. Taneda, S., "Experimental Investigation of the Wakes behind Cylinders and Plates at Low Reynolds Numbers," Journal Of The Physical Society Of Japan, Vol. 11, No. 3, pp. 302-307, March 1956.

11. Grove, A.S., et. al., "An Experimental Investigation of the Steady Separated Flow Past a Circular Cylinder," Journal of Fluid Mechanics, Vol. 19, pp. 60-86, 1964.

12. Obasaju, E.D., "An Investigation of the Effects of Incidence on the Flow Around a Square Section Cylinder," Aeronautical Quarterly, pp. 243-253

13. Chiu, W.S., and Lienhard, J.H., "On Real Fluid Flow Over Yawed Circular Cylinders", Journal of Basic Engineering, pp. 851-857, December 1967.

14. Tsuchiya, K., Ogata, S., et. al., "Karman Vortex Flow Meter," Bulletin of the Japanese Society of Mechanical Engineering, Vol. 13, No. 58, pp. 573-582, 1970.

15. Knauss, D. T., John, J. E. A., and Marks, C. H., "The Vortex Frequencies of Bluff Cylinders at Low Reynolds Numbers," Journal of Hydronautics, Vol. 10, No. 4, pp. 121-126, 1976.

16. Hoerner, S.F., Fluid-Dynamic Drag, 1965.

17. Modi, V.J., and Wiland, E., "Unsteady Aerodynamics of Stationary Elliptical Cylinders in Subcritical Flow," AIAA Journal, Vol. 8, No. 10, pp. 1814-1821, 1970.

18. Bloor, M.S., "The Transition to Turbulence in the Wake of Circular Cylinder," Journal of Fluid Mechanics, Vol. 19, 1964.

19. Ericsson, L.E., "Effect of Cross-Sectional Shape on the Response to Karman Vortex Shedding," AIAA 23rd Aerospace Sciences Meeting, January 1985.

APPENDICES

APPENDIX A

ADDITIONAL READINGS

1. Awbi, H.B., "An Assessment of the Universal Strouhal Number Concepts for Two-Dimensional Bluff Bodies," Aeronautical Journal, Vol.85, No. 850, pp. 467-469, December 1981.

2. Williamson, C.H.K., "Defining a Universal and Continuous Strouhal-Reynolds Number Relationship for the Laminar Vortex Shedding of a Circular Cylinder," The Physics of Fluids, Vol. 31, No. 10, pp. 2742-2744, October 1988.

3. Taylor, L.W., "Reducing Aerodynamic Drag of Bluff Bodies," NASA Tech Briefs, pp. 56-57, August 1990.

4. Marquart, E.J., "Numeric and Fluid Dynamic Representation of Tornadic Double Vortex Thunderstorms," Master's thesis, The University of Tennessee Space Institute, Tullahoma, August 1980.

5. Ramamurthy, A.S., et. al., "Vortex Shedding Characteristics of Eccentrically Mounted Prisms," Aeronautical Journal, pp. 42-44, January 1975.

6. Delany, N.K., and Sorensen, N.E., "Low Speed Drag of Cylinders of Various Shapes," NACA TN 3038, November 1953.

7. Okude, M., "Rearrangement of the Kármán Vortex Street," Trans. Japan Society of Aeronautical Space Science, Vol. 24, No. 64, pp.96-105, August 1981.

8. Noto, K., et. al., "Breakdown Phenomenom of the Karman Vortex Street Due to the Natural Convection," AIAA 17th Fluid Dynamics, Plasma Dynamics, and Lasers Conference, AIAA-84-1547, June 1984.

9. West, G.S., and Apelt, C.J., "The Effects of Tunnel Blockage and Aspect Ratio on the Mean Flow Past a Circular Cylinder with Reynolds Numbers Between 10^4 and 10^5," Journal of Fluid Mechanics, Vol. 114, pp. 361-377, 1982.

10. Achenbach, E., and Heinecke, E., "On Vortex Shedding from Smooth and Rough Cylinders in the Range of Reynolds Numbers 6×10^3 to 5×10^6'" Journal of Fluid Mechanics, Vol. 109, pp. 239-251, 1981.

11. Karou, A., and Weihs, D., "The Stability of Symmetrical Vortices in the Wake of Elliptical Cylinders in Confined Flow," Israel Journal of Technology, Vol. 22, pp.23-29, 1984/5.

12. Zdravkovich, M.M., "Smoke Observations of Wakes of Tandem Cylinders at Low Reynolds Numbers," Aeronautical Journal, pp. 108-114, February 1972.

13. Mujumdar, A.S., and Douglas, W.J.M., "Vortex Shedding From Slender Cylinders of Various Cross Sections," Transactions of the ASME, pp. 474-476, September 1973.

14. Okajima, A., "Strouhal Numbers of Rectangular Cylinders," Journal of Fluid Mechanics, Vol. 123, pp. 379-398, 1982.

APPENDIX B

ESTIMATED STROUHAL NUMBER UNCERTAINTY EQUATION

With the definition of Strouhal number as follows:

$$St = fd/U$$

and taking the natural log,

$$\ln(St) = \ln(fd) - \ln(U)$$

separate the variables and differentiate through,

$$\partial[\ln(St) = \ln(f) + \ln(d) - \ln(U)]$$

obtaining;

$$\partial St/St = \partial f/f + \partial d/d - \partial U/U$$

finally, the estimated uncertainty equation is determined after summing the squares of the parts and taking the square root;

$$\pm St = \sqrt{[(\partial f/f)^2 + (\partial d/d)^2 + (\partial U/U)^2]} * St$$

Bias was assumed to be zero.

VITA

Clifford Lewis Ratliff was born on July 30, 1963 in Albemarle, N.C. Cliff attended Chapel Hill High School (CHHS) in Chapel Hill, N.C. Raised in Chapel Hill, home of the University of North Carolina "Tarheels," it was only natural that he pursue basketball in high school. As a key player on the CHHS "Tigers" basketball team he and his teammates accomplished a goal set when entering high school; the N.C.-4A Basketball Championship! Cliff received the prestigious Frank Weaver Memorial Award for his outstanding leadership, continuing enthusiasm, and competitive spirit on and off the basketball court. He attended Brevard College in May 1981, where he was chosen the receipient of the Brevard College Physics Award. Prior to attending North Carolina State University (NCSU), where he was admitted into the Aerospace Engineering program in the Fall of 1983, he married Michelle M. Weisheit. Cliff graduated from NCSU on May 10, 1986 with a B.S. in Aerospace Engineering degree. Cliff and Michelle both accepted positions with Calspan Corporation/AEDC Operations in Tullahoma, TN at the Arnold AFB as a wind tunnel project engineer and computer scientist. Continuing Cliff's education he enrolled at the University of Tennessee Space Institute in the Fall of 1986 and obtained a M.S. in Aerospace Engineering degree in December 1991.